https://doi.org/10.5194/egusphere-2026-4223
Preprint. Discussion started: 28 July 2026

Surface runoff and soil evaporation dominate the sensitivity of land surface models to soil parameters

Matthias Cuntz[1,★], Stephan Thober[2,★], Anne Verhoef[3], Yijian Zeng[4], Aaron Boone[5], Agnès Ducharne[6], Sujan Koirala[7], David M. Lawrence[8], Philipp de Vrese[9], Carsten Montzka[10], Sonia I. Seneviratne[11], Harry Vereecken[10], Dani Or[12,13], Salma Tafasca[6], Naoki Mizukami[8], Rich Ellis[14], Patrick C. McGuire[15], and Lukas Gudmundsson[11]

[1]Université de Lorraine, AgroParisTech, INRAE, UMR Silva, 54000 Nancy, France
[2]Department Computational Hydrosystems, Helmholtz Centre for Environmental Research – UFZ, 04318 Leipzig Germany
[3]Department of Geography and Environmental Science, The University of Reading, Reading, United Kingdom
[4]Department of Water Resources (WRS), Faculty of Geo-Information Science and Earth Observation (ITC), The University of Twente, Enschede, The Netherlands
[5]Le Centre National de Recherches Météorologiques (CNRM), Université de Toulouse, Météo-France/CNRS, 31057 Toulouse, France
[6]Laboratory METIS, Sorbonne Université/CNRS/EPHE, 75005 Paris, France
[7]Department of Biogeochemical Integration, Max Planck Institute for Biogeochemistry, 07743 Jena, Germany
[8]NSF National Center for Atmospheric Research, Boulder, CO, USA
[9]Department of Climate Dynamics, Max Planck Institute for Meteorology, 20146 Hamburg, Germany
[10]Institute of Bio- and Geosciences: Agrosphere (IBG-3), Forschungszentrum Jülich, 52425 Jülich, Germany
[11]Institute for Atmospheric and Climate Science, ETH Zurich, Zürich, Switzerland
[12]Department of Civil and Environmental Engineering, University of Nevada Reno, Reno, NV, USA
[13]Department of Environmental Systems Science (D-USYS), ETH Zurich, Zürich, Switzerland
[14]UK Centre for Ecology and Hydrology, Wallingford, OX10 8BB, United Kingdom
[15]Department of Meteorology & National Centre for Atmospheric Science, University of Reading, Reading, United Kingdom
★These authors contributed equally to this work.

Correspondence: Matthias Cuntz (matthias.cuntz@inrae.fr) and Stephan Thober (stephan.thober@ufz.de)

Abstract. Land surface models (LSMs) are simulating land–atmosphere exchanges and are widely used in hydrology, operational weather prediction, research meteorology, and to assess land surface responses to future climate change. LSMs exhibit distinct differences in simulated water fluxes due to varying physical process representations and input land characteristics. We challenged seven state-of-the-art LSMs by altering soil hydraulic parameters from representing sand or silt to disentangle the responses of the water fluxes. The LSMs reacted differently due to complex, sometimes counter-intuitive interactions of infiltration, soil evaporation, and plant transpiration. We identified the representations of surface runoff and soil evaporation as the two main reasons behind model differences. We show how subgrid parameterization of a saturated fraction led to diverging sensitivities of runoff to soil parameters. Soil evaporation was the largest and most sensitive share of evapotranspiration in almost all models. Process parameterizations at the soil surface are identified as critical and should be improved to lead to more consistent flux partitioning. We demonstrate here that it is possible and worthwhile in model intercomparison studies to relate model results to specific process descriptions, helping users to understand model results of LSMs and helping modelling groups to identify weaknesses and move forward.

https://doi.org/10.5194/egusphere-2026-4223
Preprint. Discussion started: 28 July 2026

1 Introduction

Land surface models (LSMs) describe mathematically how energy from the sun and the sky is absorbed by plants and soils, how carbon dioxide (CO_2) is taken up and released, and how water from precipitation is first stored and then discharged from land. They have to simplify the very complex processes that are behind the fluxes into and out of the terrestrial system. LSMs are often part of larger computational model systems that represent the Earth system, which are used, among other applications, to project climate change under different scenarios of future CO_2 emissions (IPCC, 2021).

In LSMs, the world is divided into a grid of cells with varying geometries with effective surface areas corresponding to for example 50 km by 50 km. So the mathematical descriptions of the LSM have to parameterize also all the heterogeneity that exists within the 2500 km^2 grid cells in this example. Different implementations of the processes and the subgrid parameterizations across the various LSMs result in differences in calculated fluxes that contribute considerably to the spread of future climate projections (Arora et al., 2020; Müller et al., 2024).

Another contributor to the large projected range is that soil characteristics differ considerably between models (Samaniego et al., 2017; Weber et al., 2024; Weihermüller et al., 2021). There are two main sources for differences: firstly the choice of soil texture maps, and secondly the translation from soil texture information to model parameters. A variety of global maps of soil types and texture exist that all draw on field data but with very different support databases as well as underlying imputation and mapping approaches (Hengl et al., 2014; Batjes, 2016; Samaniego et al., 2019). So-called pedotransfer functions are used to infer model parameters from soil texture, however a plethora of pedotransfer functions are available, based on a range of soil supports, predominantly representative of agricultural soils (Van Looy et al., 2017; Weihermüller et al., 2021). Few studies have investigated the effects of varying soil hydraulic properties on simulated water and energy fluxes (Schweppe et al., 2022; Tafasca et al., 2020; Feigl et al., 2022), and these were limited with respect to spatial scope or the number of models used.

There has been a large number of model intercomparison projects (MIP) for LSMs with different focuses such as energy, water, or carbon fluxes (Henderson-Sellers et al., 1996; Sitch et al., 2015; Huntzinger et al., 2013; Best et al., 2015; Abramowitz et al., 2024), or evaluations on different spatial scales such as point-wise, basin-wide, or global comparisons (Chen et al., 1997; Lohmann et al., 1998; Nijssen et al., 2003; Robock et al., 1998; Friedlingstein et al., 2006; van den Hurk et al., 2016; Warszawski et al., 2014). Most of these model intercomparisons assumed that model differences are the result of differences in the model descriptions of the component fluxes (e.g. Haughton et al., 2016). However, none of these studied the effects of different process representations in detail.

Here we present results from experiments of the Soil Parameter Model Intercomparison Project (SP-MIP, Gudmundsson and Cuntz, 2017). SP-MIP aims to confront LSMs with different soil texture maps and soil parameters to determine the soil processes responsible for observed model differences. Global land-surface model simulations were conducted as part of SP-MIP with spatially constant parameters to remove correlations between climate and soil type. This enabled to reveal the effects of different process descriptions in the models.

In this study, we focus on the influence of soil hydraulic parameters on modelled water fluxes. Seven state-of-the-art LSMs were forced with the same meteorological input data. These were run with their standard configuration where each modelling

https://doi.org/10.5194/egusphere-2026-4223
Preprint. Discussion started: 28 July 2026

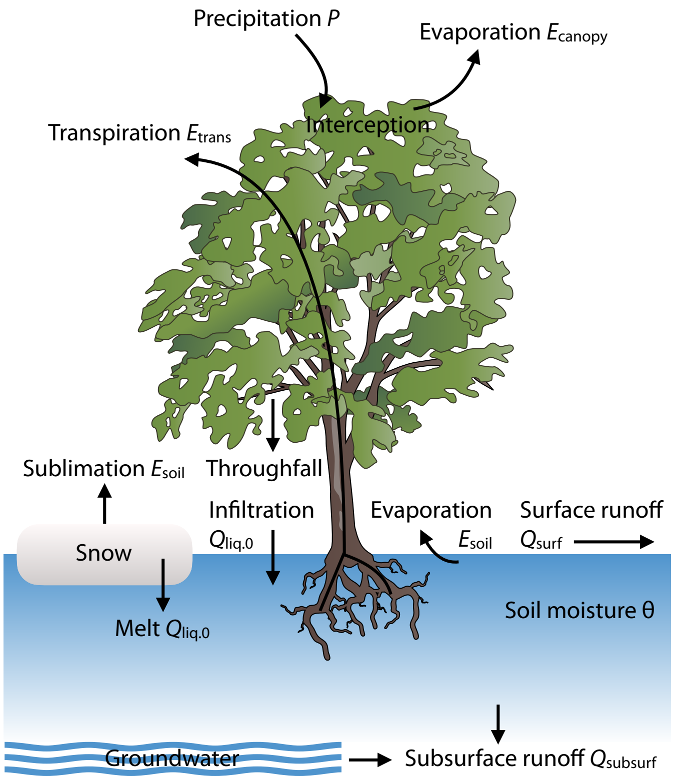

Figure 1. Water fluxes at the land surface. Conceptual overview of water fluxes at the land surface after Bonan (2008) with the notation used in this study.

group chose the soil map according to their best practises, denoted as standard run in what follows. Next, they were given globally homogeneous soil parameters representative of a sandy soil and a silty soil. While sand represents soils with very high saturated hydraulic conductivity and low water retention throughout the soil profile, silt represents soils with low saturated hydraulic conductivity and high water retention (see Material and Methods and Table 1). Looking in detail into the descriptions of the processes that lead to water fluxes at the land surface in each model allowed us eventually to reveal that surface runoff and soil evaporation are most sensitive to differences in soil properties. The parameterization of these processes consequently govern the partitioning of water fluxes in land surface models.

2 Materials and Methods

We investigated the responses of land surface models to changes in soil hydraulic parameters. The simulation design, the soil hydraulic parameters, and the participating land surface models are presented below.

https://doi.org/10.5194/egusphere-2026-4223
Preprint. Discussion started: 28 July 2026

Table 1. Soil parameters prescribed for sand and silt experiments.

Var	Description (units)	Sand	Silt
K_{sat}	saturated hydraulic conductivity ($\text{m}\,\text{s}^{-1}$)	$1.41\cdot10^{-5}$	$2.81\cdot10^{-6}$
θ_{sat}	saturated volumetric soil moisture content ($\text{m}^3\,\text{m}^{-3}$)	0.39	0.49
θ_{r}	residual volumetric soil moisture content ($\text{m}^3\,\text{m}^{-3}$)	0.05	0.05
h_{e}	air entry potential (m)	0.04	0.76
m^{BC}	Brooks-Corey m parameter	4.26	5.33
α^{vG}	van Genuchten α parameter (m^{-1})	3.48	0.66
n^{vG}	van Genuchten n parameter	1.75	1.68
Derived parameters			
λ^{BC}	Brooks-Corey λ parameter ($=5/2+2m^{\text{BC}}$)	11.02	13.16
m^{vG}	van Genuchten m parameter ($=1-1/n^{\text{vG}}$)	0.43	0.40
$\theta_{\text{fc}}^{\text{BC}}$	Brooks-Corey volumetric soil moisture content at field capacity ($h=3.3\,\text{m}$) ($\text{m}^3\,\text{m}^{-3}$)	0.17	0.38
$\theta_{\text{wp}}^{\text{BC}}$	Brooks-Corey volumetric soil moisture content at permanent wilting point ($h=150\,\text{m}$) ($\text{m}^3\,\text{m}^{-3}$)	0.10	0.21
$\theta_{\text{fc}}^{\text{BC}}-\theta_{\text{wp}}^{\text{BC}}$	Brooks-Corey volumetric plant available soil moisture content ($\text{m}^3\,\text{m}^{-3}$)	0.07	0.17
$\theta_{\text{fc}}^{\text{vG}}$	van Genuchten volumetric soil moisture content at field capacity ($h=3.3\,\text{m}$) ($\text{m}^3\,\text{m}^{-3}$)	0.10	0.29
$\theta_{\text{wp}}^{\text{vG}}$	van Genuchten volumetric soil moisture content at permanent wilting point ($h=150\,\text{m}$) ($\text{m}^3\,\text{m}^{-3}$)	0.05	0.07
$\theta_{\text{fc}}^{\text{vG}}-\theta_{\text{wp}}^{\text{vG}}$	van Genuchten volumetric plant available soil moisture content ($\text{m}^3\,\text{m}^{-3}$)	0.05	0.22
$K_{\text{fc}}^{\text{BC}}$	Brooks-Corey hydraulic conductivity at field capacity ($h=3.3\,\text{m}$) ($\text{m}\,\text{s}^{-1}$)	$1.55\cdot10^{-10}$	$7.48\cdot10^{-8}$
$K_{\text{fc}}^{\text{vG}}$	van Genuchten hydraulic conductivity at field capacity ($h=3.3\,\text{m}$) ($\text{m}\,\text{s}^{-1}\text{m}$)	$1.98\cdot10^{-10}$	$1.72\cdot10^{-8}$

https://doi.org/10.5194/egusphere-2026-4223
Preprint. Discussion started: 28 July 2026

Simulation design

We contributed with this study to the Soil Parameter Model Intercomparison Project (SP-MIP, Gudmundsson and Cuntz, 2017). SP-MIP was tailored to specifically investigate the soil component of land surface models (LSMs), i.e. the effect of varying soil hydraulic parameters related to soil water storage and transport. It follows the protocol established in the Land Surface, Snow and Soil Moisture Intercomparison Project (LS3MIP, van den Hurk et al., 2016), which was part of CMIP6 (Eyring et al., 2016) and had the goal to provide a comprehensive assessment of feedbacks between LSM parameterizations. In SP-MIP, we implemented a simulation protocol that contained seven different settings of soil parameters. Three of these settings were used in this study to understand the processes behind the responses of LSMs to varying soil parameters. The settings were firstly the LSMs' standard model setup, and secondly two settings with spatially (and vertically) constant soil hydraulic parameters. The latter two settings were chosen to cover the large range of observed hydraulic conductivity, moisture retention, and water availability to plants. One soil had high saturated hydraulic conductivity, low water retention and low storage capacity, i.e. it represented a relatively sandy soil, and the other soil had low saturated hydraulic conductivity, high water retention and high storage capacity, i.e. it represented a relatively silty soil. The soil parameters that were given to the LSM modelling groups are presented in Table 1. They correspond approximately to the values for the soils “Sand” and “Silt Loam” of Clapp and Hornberger (1978) and for the soils “Loamy Sand” and “Silt” of Schaap et al. (2001). The soil types are called “sand” and “silt” generically in this manuscript. There was no prescription of land cover data, and each modelling group used its preferred land cover map, which did not change between the three settings of different soil hydraulic parameters. The soil textures and parameters provided by SP-MIP as well as the simulation protocol can be found at Gudmundsson and Cuntz (2017).

Seven land-surface models contributed to the SP-MIP experiments. These were CLM5 (Lawrence et al., 2019), ISBA (Decharme et al., 2019), JSBACH (Hagemann and Stacke, 2015), MATSIRO (Takata et al., 2003), MATSIRO-GW (Takata et al., 2003), NOAH-MP (Niu et al., 2011), and ORCHIDEE (Tafasca et al., 2020). We provide the parameterizations of surface runoff and the description of root water uptake for each model in the Appendix. The description of surface runoff turned out to be essential to the interpretation of the results of this study. The description of root water uptake shows the difficulty to provide a *post hoc* analysis of soil-vegetation interactions and motivates the chosen proxies for a stress function for each model. All models were run from 1980 through 2010 on a spatial resolution of 0.5° x 0.5° using GSWP3 meteorological forcing, which is part of the LS3MIP protocol (Dirmeyer et al., 2006; van den Hurk et al., 2016). All simulations provided a consistent set of output variables covering the water and energy cycles following LS3MIP. Model output can be found at Cuntz et al. (2026).

Parameter sensitivity

We quantified the sensitivity of hydrologic output fluxes and state variables to modified soil hydraulic parameters. The hydrologic fluxes are evapotranspiration (E_{total}) and its sub-components canopy evaporation (E_{canopy}), soil evaporation (E_{soil}), and transpiration (E_{trans}), as well as total runoff (Q_{total}) and its sub-components surface runoff (Q_{surf}) and subsurface runoff (Q_{subsurf}). The state variable was volumetric soil moisture content (θ). The fluxes varied substantially among models and in different climates. The fluxes were hence normalized with precipitation on each grid cell to ease comparison across climates.

https://doi.org/10.5194/egusphere-2026-4223
Preprint. Discussion started: 28 July 2026

Grid cells with less than 50 mm of precipitation per year were excluded from the analyses. We then calculated model sensitivity as:

$$\Delta F/P = \frac{\overline{F}_{\text{silt}} - \overline{F}_{\text{sand}}}{\overline{P}}, \tag{1}$$

where $\overline{F}$ is the mean flux over the whole simulation period and $\overline{P}$ the mean of precipitation at the grid cell. The subscript denotes parameter settings for silty and sandy soils, respectively (Table 1).

Soil moisture, also averaged over the 30 year period, was normalized with its saturated values:

$$\Delta \frac{\theta}{\theta_{\text{sat}}} = \frac{\overline{\theta}_{\text{silt}}}{\theta_{\text{sat,silt}}} - \frac{\overline{\theta}_{\text{sand}}}{\theta_{\text{sat,sand}}}, \tag{2}$$

where θ denotes volumetric soil moisture content and θ_{sat} denotes saturated volumetric soil moisture content, i.e. porosity. Both quantities are averaged over 30 years. $\theta_{\text{sat,silt}}$ is hence the porosity of the silty soil, for example. Rooting depth and root length density are not a standard output of LS3MIP. We hence used the soil moisture content in the top 1 m of soil as a proxy for soil moisture within the root zone. We assumed root length density following Li et al. (2001) with 20% of root mass in the first 10 cm.

Low soil moisture limits plant transpiration. There is no limitation during times with high soil moisture such as during winter or during the rainy season. We hence focused on the dry seasons when looking at soil-plant interactions, i.e. in Figure 4. These were defined as the months July, August, and September from 30°S to 0° and from 30°N to 90°N, and as the months January, February, and March from 90°S to 30°S and from 0° to 30°N.

Note that we show sensitivities between silty and sandy soils, which have very different soil parameters (Table 1). Using loam instead of silt, for example, produced very similar results only with reduced absolute values.

3 Results

The diversity of simulated water fluxes

Figure 1 provides an overview of the individual water fluxes that were calculated by the land surface models (LSMs) for the standard configuration: canopy evaporation E_{canopy}, transpiration E_{trans}, soil evaporation E_{soil}, surface runoff Q_{surf}, and subsurface runoff Q_{subsurf}. Canopy evaporation E_{canopy} represents all precipitation, rain and snow, that is intercepted by vegetation and which is subsequently evaporating from the plant surfaces. Transpiration E_{trans} represents all water that passes through plants, that means is taken up by roots from the soil, ascends through plant xylem, and is transpired through stomata in the plant leaves. On a global scale, soil evaporation E_{soil} includes all water evaporated and sublimated to the atmosphere that is neither E_{canopy} nor E_{trans}. This includes evaporation from the soil surface layer and evaporation from wetlands or other water bodies. Total evapotranspiration E_{total} is the sum of E_{canopy}, E_{trans}, and E_{soil}. Surface runoff Q_{surf} includes the water that runs on top of the land surface if it cannot infiltrate either because the soil is already saturated (saturation-excess or Dunne runoff), or because it rains more than the soil allows to infiltrate (infiltration-excess or Horton runoff). The two processes happen conceptually in LSMs often in different parts of a grid cell, i.e. there is a part of the grid cell that is already saturated and

https://doi.org/10.5194/egusphere-2026-4223
Preprint. Discussion started: 28 July 2026

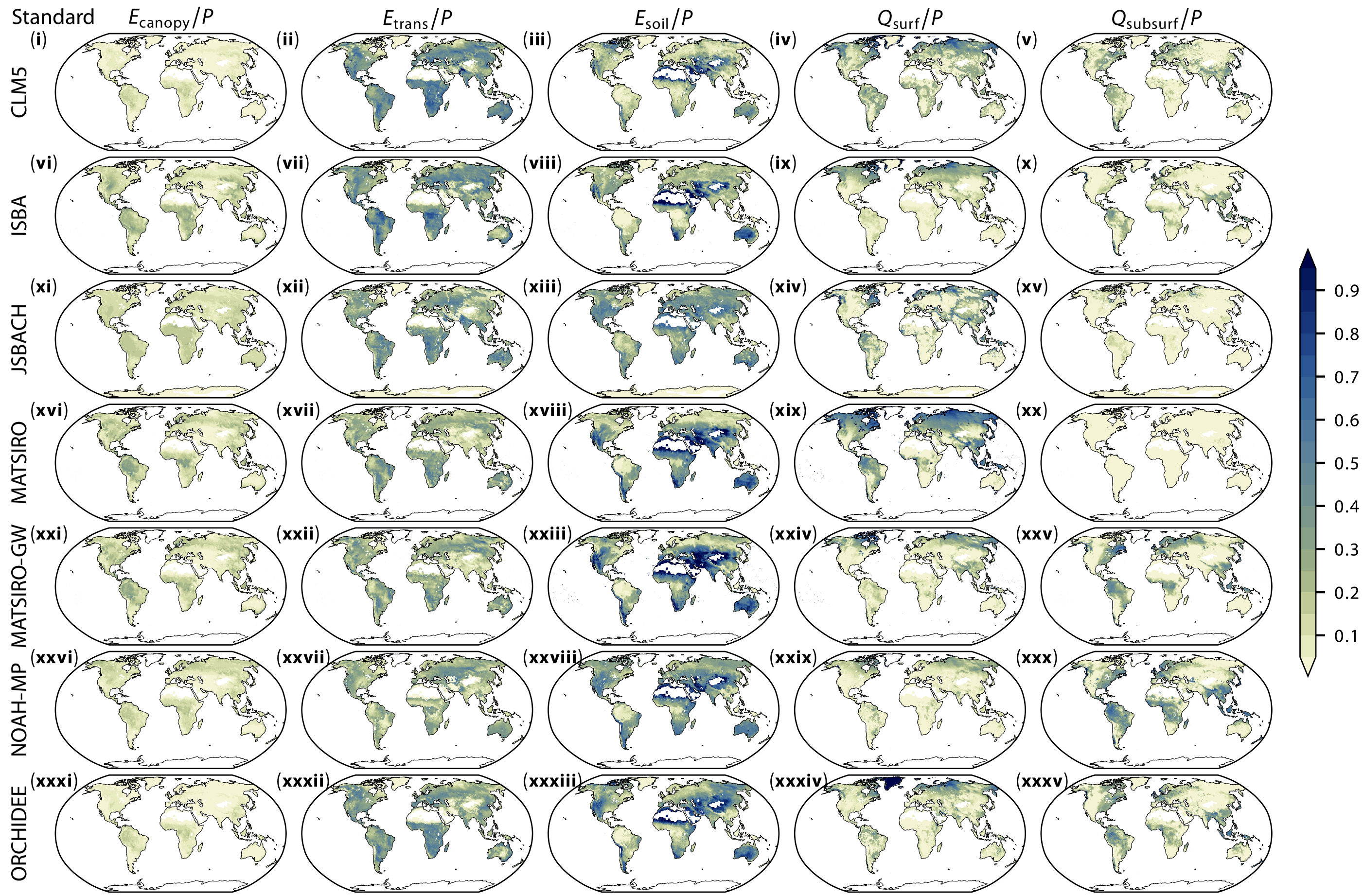

Figure 2. Individual water fluxes at the land surface over precipitation for the model's standard runs. Precipitation is partitioned into interception with consequent canopy evaporation E_{canopy} (1st column), transpiration E_{trans} (2nd column), soil evaporation E_{soil} (3rd column), surface runoff Q_{surf} (4th column), and subsurface runoff Q_{subsurf} (5th column). Precipitation water can also be stored in soil and snow. This is temporary in most places so that the mean fluxes over incoming precipitation for 1981-2010 sum up to one at each grid cell for each model (row). Cells with a mean annual precipitation of less than 50 mm were excluded.

saturation-excess runoff can occur, and there is a part of the grid cell that is not saturated and infiltration-excess runoff can happen (see Appendix). Soil freezing, which is not represented in all LSMs, can also alter infiltration and infiltration-excess runoff. Water reaching the soil surface can be precipitation directly (throughfall), dripped from the plant canopy, or water from snow melt. Subsurface runoff Q_{subsurf} finally represents all water that leaves the system after passing through the soil. This is mainly vertical flow in LSMs. Some models also include a storage to represent groundwater. All hydrologic processes on the land surface are represented in the two parameterizations of Q_{surf} and Q_{subsurf} alone. Lateral flow such as interflow on hill slopes is included rather implicitly in LSMs. Ponding of water in puddles, ponds, and similar is not included in all LSMs.

The individual water fluxes for runs with the standard configuration of each model within SP-MIP are presented on Figure 2. They are given as a fraction of precipitation at each grid cell for better comparison of different climate regions. One can see similarities between LSMs as well as large differences between them on the individual fluxes. For example, transpiration E_{trans} over precipitation P is generally larger than soil evaporation E_{soil}/P in cold humid regions (see Figure A5 for climate regions). In dry regions such as Southern California, there can be as much E_{trans} as E_{soil} in some models like CLM5, or the surface-to-atmosphere flux is dominated by E_{soil} as in the MATSIRO models. There are only two out of seven LSMs, CLM5 and ISBA, that have larger E_{trans}/P than E_{soil}/P globally (Table 2) and only CLM5 has a transpiration fraction $E_{\mathrm{trans}}/E_{\mathrm{total}}$ greater than 0.5, which in line with observation-based estimates of about $57\% \pm 7\%$ (Wei et al., 2017). It is worth noting that even in dry lands, which account for about 40% of global land, E_{soil} and E_{trans} are roughly equal (Sun et al., 2019). Globally, total evapotranspiration E_{total} is generally larger than total runoff Q_{total} in all models (Figure A1 and Table 2), similar to independent estimates of the global water cycle (Rodell et al., 2015). Q_{total} is only about one fourth of precipitation P for ISBA and JSBACH, and about one third in the other models. The exceptions are hot humid and cold dry regions where Q_{total}/P can reach values as large as E_{total}/P in all models. While E_{trans} and E_{soil} have about the same magnitude in large regions of the world (cf. also left column of Figure A2), there is a clear dichotomy between Q_{surf} and Q_{subsurf}. While CLM5 has similar amounts of Q_{surf} and Q_{subsurf} in the Amazon, Europe, and south-east Asia (Figure 2 iv and v), other models have either Q_{surf} or Q_{subsurf} dominating single grid points. This goes as far as JSBACH and MATSIRO having almost only Q_{surf}, while NOAH-MP is the only model where the global mean fraction of Q_{subsurf} is larger than the global mean fraction of Q_{surf} (Table 2).

Sensitivity of fluxes to soil hydraulic parameters

The reason behind the large differences of hydrologic fluxes between LSMs was hypothesized to stem from large differences in soil characteristics employed by the models (e.g. Samaniego et al., 2017; Weber et al., 2024; Weihermüller et al., 2021). Tafasca et al. (2020) had, however, found that soil texture maps had limited influence on water fluxes in ORCHIDEE. However, over large parts of the globe there is good agreement in soil texture between the various soil maps available to land surface modellers. Hence, Tafasca et al. found larger changes in areas where the maps had diverging soil types. We tested this by forcing LSMs with globally uniform soil parameters and analysing only the differences between simulations performed with each model and different soil maps to limit influences of covariation between soil and other variables such as vegetation type (Freschet et al., 2018). We choose soils with very different hydraulic properties (Table 1) to maximize the effects. We use the generic names of *sand* and *silt* to refer to these soils from here on (cf. Material and Methods). The differences (Δ) between results with silty soil

https://doi.org/10.5194/egusphere-2026-4223
Preprint. Discussion started: 28 July 2026

and results with sandy soil (i.e. $\Delta F = F_{\text{silt}} - F_{\text{sand}}$) are shown in Figure 3 for the individual fluxes normalized by precipitation P and aggregated to five broad climate zones. The five climate zones range from hot to dry climates and combine several climate regions of the Köppen-Geiger classification (Beck et al., 2023). Maps of the Köppen-Geiger classification and the aggregated SP-MIP regions are given in Figure A5.

The first row of Figure 3 shows very well how strongly the return of precipitation to the atmosphere (i.e. evapotranspiration) depends on soil type. In general, models show higher E_{total} for silt in comparison to sand (with the exception of JSBACH for cold dry climate), but there is no apparent pattern with respect to model or climate. The response of E_{total} is the combined effect of E_{trans} and E_{soil}. Both, E_{soil} and Q_{subsurf} are consistent among all models and the direction of change is as expected. In detail, a silty soil has smaller hydraulic conductivity than a sandy soil and hence less Q_{subsurf}. The same effect leads to higher E_{soil} for a silty soil in comparison to a sandy soil. Notably, the absolute magnitude of changes, expressed as a fraction of P, are very high for E_{soil}.

In contrast, changes in Q_{surf} are less consistent. Changes in Q_{surf} can be both positive and negative ranging from -0.2 to about 0.2 for cold dry climates for MATSIRO-GW and NOAH-MP, respectively. From theory, it would be expected that changes are positive (as they are for NOAH-MP and ORCHIDEE and with smaller magnitude also for JSBACH) because a sandy soil can infiltrate more water than a silty soil. All models but NOAH-MP and ORCHIDEE use saturated area fraction concept (f_{sat} Beven and Kirkby, 1979) to separate infiltration from surface runoff. f_{sat} is directly related to the amount of soil moisture in the root zone (e.g. JSBACH, ISBA) or the water table depth (CLM5, MATSIRO, MATSIRO-GW, cf. Appendix). The latter models tend to show a decrease in Q_{surf}, because the water table is higher in these models for sand compared to silt. CLM5 has a zero flux boundary condition at the bottom of the soil column (Lawrence et al., 2019). The K_{baseflow} parameter determining how fast the water table is decreasing has remained unchanged. MATSIRO-GW shows the largest changes in Q_{surf} for all climate zones, distinctly different than other models. It is the only model having an explicit groundwater storage which depends on aquifer properties (Koirala et al., 2010). These properties remain unchanged and apparently lead to an enhanced effect by changed soil parameters.

While the Q_{surf} parameterizations depend directly on soil parameters, changes in E_{trans} are a downstream effect because water that transpires has to first infiltrate and not be evaporated (Lehmann et al., 2019). E_{trans} shows very little changes for all climates, apart from hot dry. For this climate, all models show strong decreases ranging from -0.05 for CLM5 to -0.2 for MATSIRO. In general, simulated transpiration can be limited by soil moisture if the latter is below a model-dependent threshold (i.e. field capacity in most models, cf. Appendix). For cold climates, both humid and dry, NOAH-MP and ORCHIDEE show decreases of E_{trans} of more than -0.1, whereas the other models show almost no change. These are the only two models that do not use f_{sat} to calculate Q_{surf}, which results in higher Q_{surf} for silt in comparison to sand in these climates. This leads again to a higher soil water limitation in silty soil (similarly as for hot dry climates) and as a result to negative differences for E_{trans}. We expand on the effect of soil texture on soil water limitation for E_{trans} in the next section.

https://doi.org/10.5194/egusphere-2026-4223
Preprint. Discussion started: 28 July 2026

Table 2. Global mean of the fractions of the individual water fluxes canopy evaporation E_{canopy}, transpiration E_{trans}, soil evaporation E_{soil}, surface runoff Q_{surf}, and subsurface runoff Q_{subsurf} over precipitation P, the ratio of transpiration E_{trans} to total evapotranspiration E_{total}, and E_{total} over P in the models standard run (Std), and the runs with sandy soil (Sand) and silty soil (Silt). Q_{total} is $1-E_{\text{total}}/P$. The spatial distributions of the values are shown in Figure 2 and Figures A3 and A4 for standard, sandy, and silty soils, respectively, and in Figure A1 for E_{total}/P.

	E_{total}/P Std/Sand/Silt	E_{canopy}/P Std/Sand/Silt	E_{trans}/P Std/Sand/Silt	E_{soil}/P Std/Sand/Silt	Q_{surf}/P Std/Sand/Silt	Q_{subsurf}/P Std/Sand/Silt	$E_{\text{trans}}/E_{\text{total}}$ Std/Sand/Silt
CLM5	0.67/0.61/0.72	0.05/0.06/0.05	0.37/0.37/0.36	0.25/0.18/0.31	0.19/0.20/0.17	0.12/0.19/0.10	0.54/0.60/0.50
ISBA	0.74/0.68/0.74	0.13/0.11/0.11	0.33/0.34/0.32	0.28/0.23/0.31	0.14/0.16/0.14	0.10/0.14/0.11	0.44/0.49/0.43
JSBACH	0.70/0.63/0.63	0.12/0.12/0.12	0.27/0.37/0.36	0.31/0.14/0.15	0.15/0.16/0.21	0.05/0.10/0.05	0.34/0.50/0.50
MATSIRO	0.68/0.65/0.68	0.11/0.12/0.11	0.22/0.27/0.20	0.35/0.26/0.37	0.32/0.33/0.31	0.01/0.03/0.00	0.30/0.38/0.28
MATSIRO-GW	0.83/0.59/0.78	0.11/0.11/0.11	0.22/0.24/0.21	0.50/0.24/0.46	0.15/0.21/0.12	0.14/0.18/0.13	0.30/0.38/0.28
NOAH-MP	0.68/0.56/0.69	0.09/0.10/0.09	0.22/0.25/0.17	0.37/0.21/0.43	0.10/0.03/0.11	0.22/0.42/0.20	0.32/0.44/0.26
ORCHIDEE	0.68/0.65/0.68	0.05/0.05/0.04	0.29/0.27/0.16	0.34/0.33/0.48	0.16/0.06/0.14	0.15/0.29/0.18	0.43/0.43/0.27
Mean	0.71/0.62/0.70	0.10/0.10/0.09	0.27/0.30/0.26	0.35/0.23/0.36	0.17/0.16/0.17	0.11/0.19/0.11	0.38/0.46/0.36

Soil water limitation on transpiration

Previous sections have shown that there was relatively little change of transpiration ΔE_{trans} in most regions when changing soil type with the exception of hot dry climates. In this climate, plant transpiration and carbon uptake is limited by large soil water deficits. Also for hot humid and temperate climates, there are dry seasons and we hence zoom into these seasons in Figure 4. Soil water limitation of plant activity is often implemented with a so-called stress factor f_{stress} in land surface models, which is applied either to stomatal conductance or to photosynthetic activity or to both (see e.g. Egea et al., 2011, cf. also Appendix). NOAH-MP, for example, uses the plant available water in the root zone for f_{stress} (Niu et al., 2011, and Figure 4U), which is the amount of water above the wilting point relative to the maximum amount of water between field capacity and wilting point. f_{stress} is defined as the inverse of field capacity θ_{fc} and decreases linearly to zero at the wilting point θ_{wp}. f_{stress} has different forms and complexities in the LSMs. f_{stress} of ISBA, for example, looks similar to NOAH-MP at first sight with the difference that the sum of water in the soil layers is weighted by root length density and that f_{stress} is one above a threshold (cf. Appendix), linearly decreasing to zero at θ_{wp}. However, ISBA also differentiates between short and tall vegetation as well as between isohydric and anisohydric plant strategies. It is further not applying f_{stress} directly on stomatal conductance but on the relative CO_2 concentration within the stomatal cavity (Calvet et al., 2004). We calculated proxies of f_{stress} for each of the models based on the way f_{stress} is calculated in each of them (see Appendix). The Δf_{stress} proxies show mainly the same spatial patterns than ΔE_{trans} but the magnitudes can differ significantly (Figure 4 right column), as Δf_{stress} mostly accentuates areas of water limitation.

https://doi.org/10.5194/egusphere-2026-4223
Preprint. Discussion started: 28 July 2026

Transpiration E_{trans} of the dry seasons decreases in large areas when changing from sandy to silty soils (Figure 4 left column), especially in drylands where the decrease in $\Delta E_{\text{trans}}/P$ exceeds 0.2 in most models. MATSIRO, NOAH-MP, and ORCHIDEE show also large decreases in the very cold regions of the high latitudes. Concurrently, almost all models show a widespread increase in the 1-metre soil saturation (Figure 4 middle column), but with very different magnitudes for the individual models. Only JSBACH shows a very slight tendency of reduced soil saturation with silty soil than with sandy soil. A silty soil can generally hold more water over a longer period than a sandy soil. However, most SP-MIP models use the difference of volumetric soil moisture content (generically called soil moisture in the following) at field capacity and wilting point as the threshold where transpiration starts to be limited by soil moisture (cf. Appendix). Both, field capacity and wilting point change substantially between sandy and silty soils (Table 1). The change in plant water limitation in the models can thus be negative indeed when changing from sand to silt even with higher soil saturation. For ISBA, the MATSIRO models, NOAH-MP, and ORCHIDEE, there are large areas on Earth with higher relative soil saturation but less transpiration in silty than in sandy soils.

CLM5 was the only model in the SP-MIP ensemble that included a full soil-plant hydraulic model, where root water uptake depends on the difference between root and soil water potentials, and on soil hydraulic conductivity (Kennedy et al., 2019). There is hence no f_{stress} in CLM5 but plant water limitation depends directly on soil hydraulic conductivity. The model can adjust the water potentials in the plants so that water supply suffices demand, which means that it can move root water uptake to deeper soil layers if the topsoil dries out. E_{trans} of CLM5 was hence rather insensitive to changes in soil texture. Models using f_{stress} also take up water from deeper soil layers once the upper layers dry out, but the deeper soil water uptake cannot compensate for the lack of root water uptake in the upper layers. These models showed hence a more pronounced response of E_{trans} and f_{stress} to changes in soil texture.

4 Discussion

All land surface models (LSMs) that participated in SP-MIP use the Richards equation to calculate soil water transport (Richards, 1931), and all-but-one model [ISBA used the semi-empirical model of Jacobs (1994)] used the so-called Farquhar model for describing photosynthesis (Farquhar et al., 1980). The models differ, however, substantially in the other process descriptions such as how soils exert water limitation on transpiration or how surface runoff is estimated (cf. Appendix). Q_{surf} represents in some models saturation-excess as well as infiltration-excess runoff, while it encodes only infiltration-excess runoff in others. However, Q_{surf} and Q_{subsurf} together (Q_{total}) is the amount of water that is not returned to the atmosphere in the long term (E_{total}), which should be not too different between LSMs to minimize atmospheric biases when coupled to atmospheric models. Or, E_{soil} can be envisaged as evaporation from the soil surface layer in LSMs. This can be from a separate bare-soil fraction and/or from soil underneath vegetation depending on the LSM. E_{soil} is encoded very differently in the different LSMs. But it is conceptually all water evaporated that is neither E_{canopy} nor E_{trans}, the two being well defined. E_{soil} includes thus evaporation from wetlands or other water bodies, for example, that are or are not represented explicitly in the LSMs. E_{total}

https://doi.org/10.5194/egusphere-2026-4223
Preprint. Discussion started: 28 July 2026

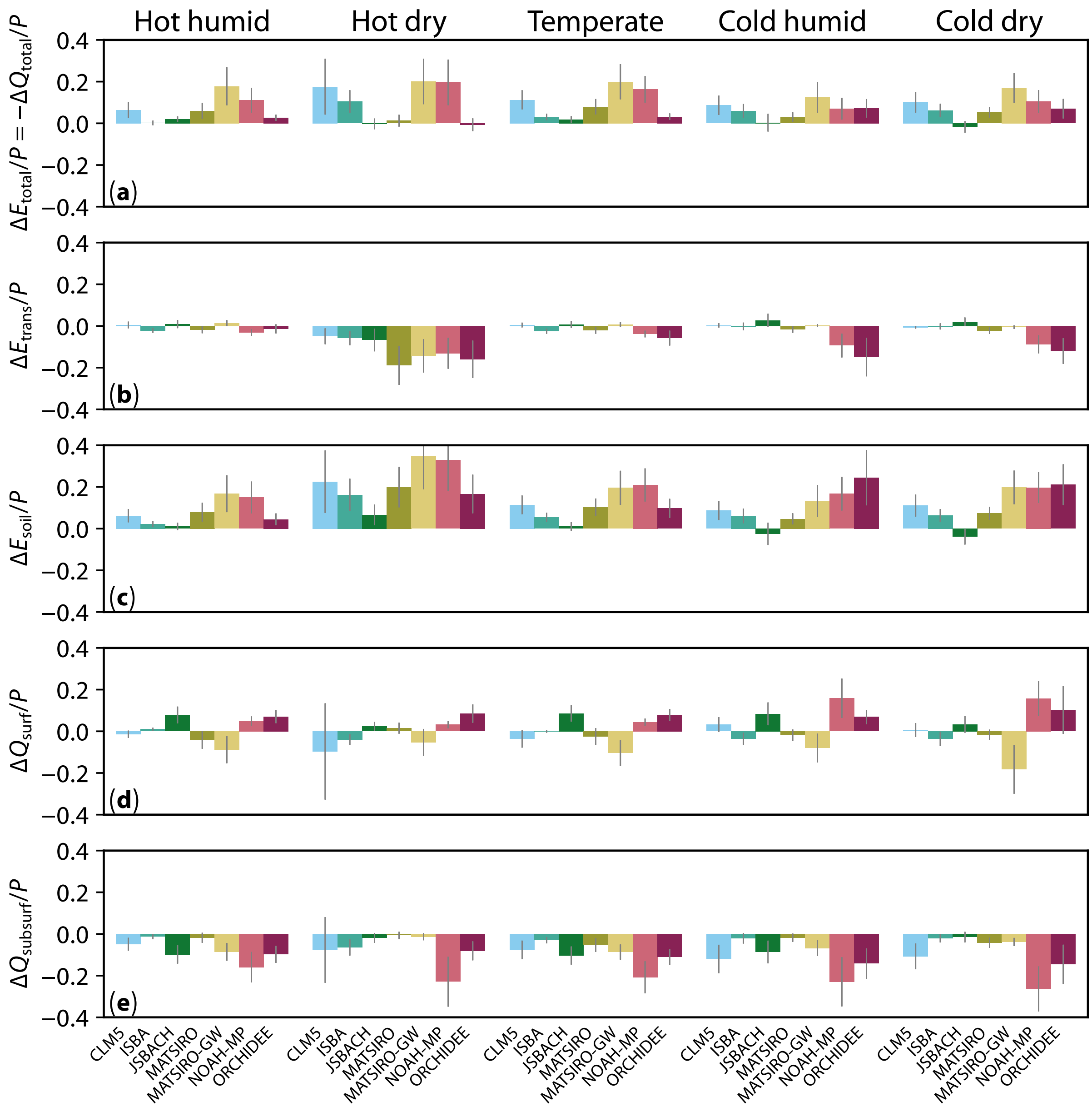

Figure 3. Mean differences of water fluxes over precipitation between the silt and sand experiments for SP-MIP climate regions. Difference (Δ) of mean evapotranspiration E_{total} over incoming precipitation P for 1981-2010 of the experiment silt minus the experiment sand for each model in each SP-MIP climate region (cf. Figure A5) (**a**) as well as the component fluxes transpiration E_{trans} over P (**b**), soil evaporation E_{soil} over P (**c**), surface runoff Q_{surf} over P (**d**), and subsurface runoff $Q_{subsurf}$ over P (**e**). Water storage has no long-term trend if the LSM is run into steady state. If more water is lost by evapotranspiration, this water is missing for runoff and hence $\Delta Q_{total}/P = -\Delta E_{total}/P$, which can be seen in Figures A6 and A7. Note that the mean of the individual fractions of each grid cell of Figures A6 and A7 are given rather than the ratio of the mean fluxes over mean precipitation.

https://doi.org/10.5194/egusphere-2026-4223
Preprint. Discussion started: 28 July 2026

should, again, be similar between the LSMs. There are hence different concepts behind the process descriptions in different LSMs but the summary fluxes E_{canopy}, E_{trans}, E_{soil}, Q_{surf}, and Q_{subsurf} should represent similar water fractions in all LSMs.

There were basically only two coherent results between models when changing soil texture from a sandy soil to a silty soil: all models showed an increase in soil moisture and also an increase in soil evaporation E_{soil}. We identified the descriptions of the two processes soil evaporation E_{soil} and surface runoff Q_{surf} as the main drivers of the large variability of model sensitivity to changed soil hydraulic parameters.

Soil evaporation and transpiration

There is an extensive literature with several reviews that compare point-scale estimates of the proportion of transpiration on total evapotranspiration ($E_{\text{trans}}/E_{\text{total}}$) with satellite-derived estimates, isotope-based estimates, and model results (Schlesinger and Jasechko, 2014; Wang et al., 2014; Bowen et al., 2019; Nelson et al., 2020). They converge on the global average of $E_{\text{trans}}/E_{\text{total}}$ being approximately between 50% and 70% depending on vegetation density among others (Wei et al., 2017). The SP-MIP models with the highest ratios, i.e. CLM5, ISBA, and ORCHIDEE, have between 43% and 54% $E_{\text{trans}}/E_{\text{total}}$ in their standard runs (Table 2) while the other SP-MIP models have only around 30%. This mirrors the large spread in CMIP5 models, which were generally between 30% and 50% (Berg and Sheffield, 2019). Studies such as Lian et al. (2018) have concluded that the underestimation of $E_{\text{trans}}/E_{\text{total}}$ in CMIP5 models comes from the descriptions of plant processes in the land surface models, using a machine-learning model with mainly above-surface variables, while other authors (e.g. Chang et al., 2018) were focusing rather on soil process descriptions to investigate the cause of the underestimation of $E_{\text{trans}}/E_{\text{total}}$.

Silty soils hold generally more water than sandy soils over a longer period (cf. $\theta_{\text{fc}} - \theta_{\text{wp}}$ in Table 1). This should lead to larger soil evaporation E_{soil} in silty soils, which is indeed observed in all SP-MIP models (Figure 3 and Table 2). The magnitude of the change, i.e. ΔE_{soil}, was, however, very large in the models and it was dominating ΔE_{total}. E_{soil} had the most sensitive parameters from all process descriptions in earlier studies of NOAH-MP (Cuntz et al., 2016) and CLM4.5 (Göhler et al., 2013). One parameter for E_{soil} (w in Eq. A25) was so prominent in NOAH-MP, for example, that it was used as the single parameter to calibrate NOAH-MP's long-term water balance. NOAH-MP compared then very well with more specialized hydrologic models for streamflow predictions within Europe without changing any other model parameter (Samaniego et al., 2019). The parameterization of E_{soil} changed substantially in CLM5 where water diffuses through a dry surface layer before emanating from the soil (Swenson and Lawrence, 2014). However, CLM5 is sensitive to changes in soil hydraulic parameters in some regions even though to a lesser extent than other SP-MIP models (Figure 4).

Soil evaporation E_{soil} is indeed a large quantity in the SP-MIP models. It is larger than E_{trans} in all models but CLM5 and ISBA (Table 2). E_{soil} comes exclusively from evaporation from non-vegetated surfaces in the former models so that it is sensitive to the definition of the bare soil fraction within a grid cell or within grid cell patches. There is in reality, however, not much bare soil fraction in the humid regions of the world because bare soil gets quickly colonized by grasses and forbs. E_{soil} in CLM5 includes evaporation from underneath the vegetation, for example from the forest floor (Lawrence et al., 2018). ISBA uses a hybrid approach between bare-soil and below-canopy evaporation (Boone et al., 2017), which increased $E_{\text{trans}}/E_{\text{total}}$

https://doi.org/10.5194/egusphere-2026-4223
Preprint. Discussion started: 28 July 2026

compared to an approach using purely bare-soil fraction for E_{soil}. It was shown that ISBA would increase $E_{\text{trans}}/E_{\text{total}}$ even more if it used the mechanistically-based parameterization of soil evaporation from CLM5 (Martí et al., 2025).

In areas with large vegetation fractions such as in hot humid regions, our analysis showed that models using E_{soil} solely from bare soil fractions are much more sensitive to changes of soil hydraulic parameters than models where E_{soil} happens also on vegetated areas. E_{soil} of the latter models are also sensitive to changes of soil hydraulic properties in drier, less vegetated regions. As E_{soil} is overall very large, it cannot simply be improved by more appropriate soil parameters. It seems that the concept of bare-soil fraction should be revisited and that more appropriate process descriptions should be included in the LSMs. For example, vapour transport in the description of water flow and redistribution in soil (via the Richards equation) could be included so that soil evaporation is calculated directly rather than parameterized (Haverd and Cuntz, 2010; Zeng et al., 2011; Chang et al., 2018; Cuntz and Haverd, 2018; Garcia Gonzalez et al., 2012). A litter layer is also rarely included in current LSMs while it strongly inhibits soil evaporation (Ogée and Brunet, 2002; Napoly et al., 2017). These are complex changes for large-scale LSMs and would require substantial work, but need to be done to improve the partitioning of E_{total} into evaporation and transpiration.

Runoff

The SP-MIP models generally computed a large fraction of surface runoff (Q_{surf}) compared to subsurface runoff (Q_{subsurf}). The magnitude and extent depended on the regions and on the model (Figure 2 and Table 2). Studies have shown, however, that there is only limited direct surface runoff, being less than 40% at maximum in river catchments (Jasechko et al., 2016; Hare et al., 2021). Given the large fraction of Q_{surf} in the SP-MIP models, one would expect also large changes of surface runoff when changing from sandy to silty soils. Our hypothesis was that silty soils can infiltrate water less easily than sandy soils, hence having more Q_{surf}, that silty soils have higher water retention and lower hydraulic conductivity than sandy soils and thus have less Q_{subsurf}, and that as a result silty soils would also have more soil moisture stored than sandy soils. Confirming our hypothesis, subsurface runoff was decreased on silty soils in all models, with quite extensive differences in magnitude across models and regions (Figure 3e and Figure A7 right column). Surface runoff on silty soils was, however, only larger than on sandy soils in JSBACH, NOAH-MP, and ORCHIDEE. Contrary to our hypothesis, CLM5 and the MATSIRO models had even less Q_{surf}, hence more infiltration, on silty soils than on sandy soils (Figure 3d). This comes from the fact that all models but NOAH-MP and ORCHIDEE included the notion of subgrid surface runoff via the concept of saturated area fraction (f_{sat}, see Appendix). Subgrid surface runoff was introduced in a large number of land surface models after the Red–Arkansas River basin experiment (Liang et al., 1998; Lohmann et al., 1998; Wood et al., 1998) of the Project for Intercomparison of Land surface Parameterization Schemes (PILPS Henderson-Sellers et al., 1996), which had highlighted deficiencies in river runoff and evapotranspiration. This could not be improved by changes to Q_{subsurf} alone. Q_{subsurf} out of several meter thick soils tended to be too dampened and with a long phase lag relative to precipitation. A subgrid parameterization was thus introduced so that part of the grid cell such as river valleys could be saturated (f_{sat}), on which saturation-excess (Dunne) runoff could happen. There is no infiltration in this saturated fraction and the saturation-excess runoff is hence not following our hypothesis above. Total surface runoff becomes then sensitive to f_{sat} and how it is parameterized, and it can lead to the counter-intuitive effect

https://doi.org/10.5194/egusphere-2026-4223
Preprint. Discussion started: 28 July 2026

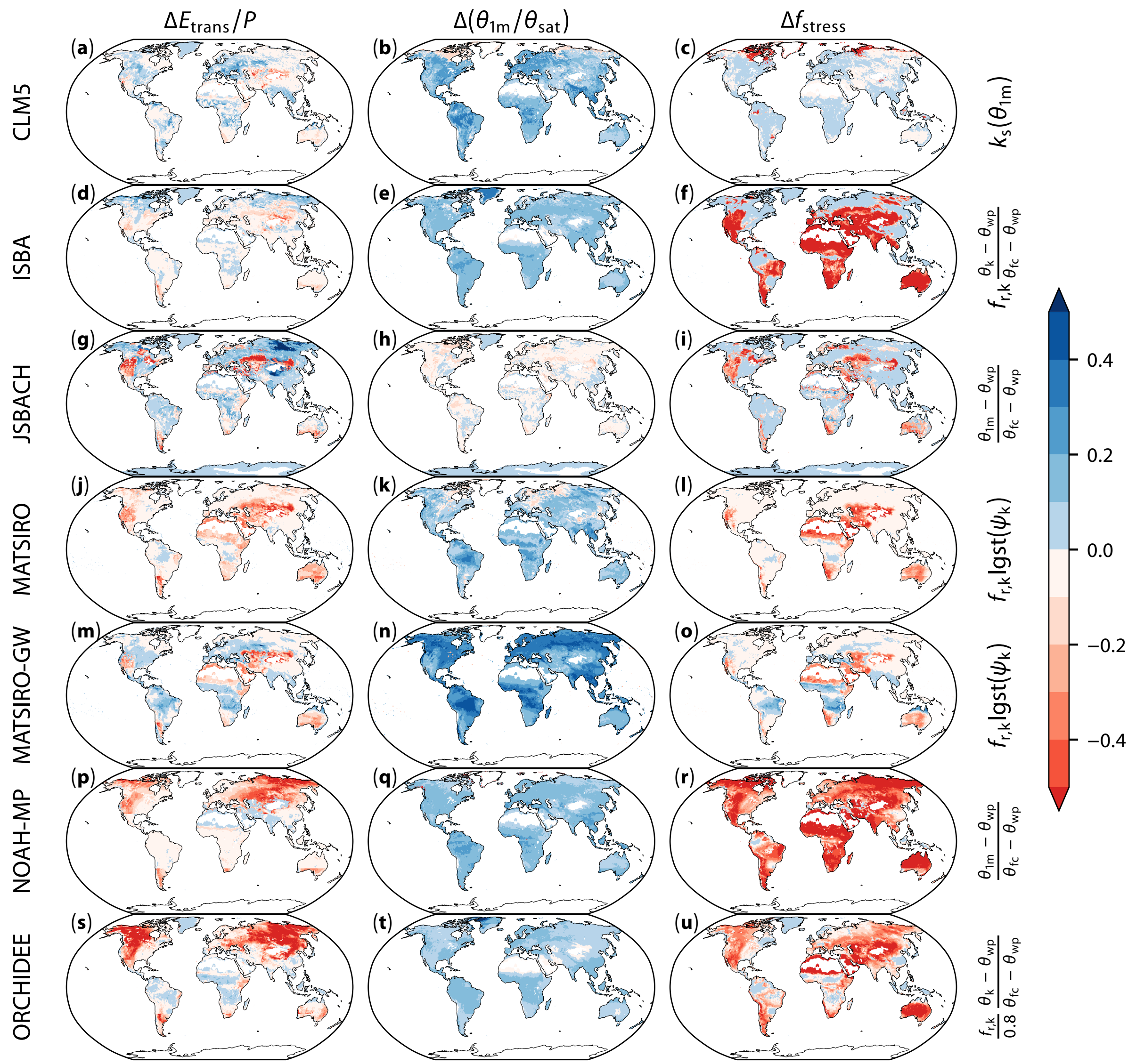

Figure 4. Differences of transpiration-related variables for dry seasons between silt and sand experiments. Differences (Δ) of transpiration E_{trans} of the dry season (1st column) over mean incoming precipitation P of 1981-2010 of the silt minus the sand experiment for each model (row), differences of ratios of mean volumetric soil moisture content of the first meter $\theta_{1\mathrm{m}}$ over saturation soil moisture content θ_{sat} (2nd column), and differences of post-processed stress factors that reflect the descriptions of soil moisture limitation on plant activity in the individual models (3rd column). The right labels of each column give codified forms of the stress factors in each model. The full description of the connection between soil water and transpiration is given in the Appendix for each model. The stress factor f_{stress} is lower for stronger limitations of transpiration. The difference of stress factors $\Delta f_{\mathrm{stress}}$ between silt and sand experiments (i.e. silt minus sand) is hence negative if there is reduced E_{trans} in silty compared to sandy soils. To better emphasize stress, dry season averages are presented here, where the dry season is summer in the extra-tropics and winter in the tropics. That means dry season is July, August, and September for $-30°$ to $0°$ and $30°$ to $90°$, and January, February, and March for $-90°$ to $-30°$ and $0°$ to $30°$. Note the scale difference to the annual mean values of $\Delta E_{\mathrm{trans}}$ of Figure A7.

https://doi.org/10.5194/egusphere-2026-4223
Preprint. Discussion started: 28 July 2026

that there is less surface runoff on silty than on sandy soil such as in CLM5 and the MATSIRO models. Vereecken et al. (2019) touched on the importance of f_{sat} for total runoff generation, which we here confirm with the SP-MIP experiments.

Two main approaches are followed in the SP-MIP models to parameterize f_{sat}: 1. f_{sat} depends on the mean water table depth of the grid cell as in CLM5 and the MATSIRO models, or 2. it depends on root zone soil moisture as in ISBA and JSBACH. See Appendix for details. Both approaches can lead to large saturated fractions. For the models of the first category, they tend to have shallower water table depths in sandy soils than in silty soils because water percolates more easily in sandy soils with lower water retention and higher hydraulic conductivity than in silty soils. Water accumulates either above the bedrock in CLM5 (Lawrence et al., 2019) or in the groundwater reservoir in MATSIRO-GW (Koirala et al., 2010). Both cases lead to deeper water table depths in silty soils than in sandy soils, hence smaller saturated surface fractions, and thus decreased surface runoff on silty soils compared to sandy soils.

For the models of the second category, that relate f_{sat} to root zone soil moisture, larger soil saturation leads to larger f_{sat} and hence larger Q_{surf}. Soil saturation was higher in silty than in sandy soils in all models but JSBACH (Figure 4 middle column). Surface runoff coming from the saturated fraction should hence be larger in silty soils than in sandy soils, the same direction as on the unsaturated fraction. The magnitude in saturation changes was low in ISBA so that f_{sat} and thus Q_{surf} did not change much between model experiments. Soil saturation was almost the same for sandy and silty soils in JSBACH with a slight tendency to lower soil saturation in silty soils (Figure 4). Q_{surf} of JSBACH did, however, respond rather strongly to changes in soil parameters which is in accordance with our hypothesis. It is likely that f_{sat} was smaller in JSBACH than in the other models, due to the use of the standard deviation of terrain height in the calculation of f_{sat} (cf. Appendix), but f_{sat} has unfortunately not been an output variable in the LS3MIP protocol, which was used in SP-MIP (Gudmundsson and Cuntz, 2017).

NOAH-MP and ORCHIDEE did not use the concept of saturated water fraction. With the chosen option (original NOAH), NOAH-MP simply checks if there is pore volume available in the root zone to fill with water. This could be seen as a maximum possible infiltration approach. NOAH-MP had hence the smallest Q_{surf} and also the largest $Q_{subsurf}$ of all SP-MIP models. ORCHIDEE uses hydraulic conductivity to calculate infiltration. It is not using hydraulic conductivity of the first, potentially dry soil layer but the mean of the hydraulic conductivities of the first saturated soil layer and the layer just above. ORCHIDEE also ponds water in case of saturated conditions, which further increases infiltration because water can infiltrate over several time steps, which is opposite to approaches using f_{sat} (Vereecken et al., 2019). This led in both models, NOAH-MP and ORCHIDEE, to higher amounts of infiltration in sandy than in silty soils and led in consequence to more Q_{surf} on silty soils, as hypothesized.

Therefore, how models parameterize infiltration matters. The models are certainly sensitive to the use of the concept of a saturated water fraction but they are even more sensitive to the specific implementation of f_{sat}. Using water table depth in f_{sat} can lead to desired behaviours such as reduced subsurface runoff in MATSIRO-GW compared to MATSIRO but can also behave counter-intuitively as in this study where there was less surface runoff on silty soils compare to sandy soils, all other conditions being equal. It would be interesting to know if the reduced subsurface runoff in MATSIRO-GW comes almost solely from the effect that water table depth has on f_{sat}, and how much do other details of the groundwater implementation in

https://doi.org/10.5194/egusphere-2026-4223
Preprint. Discussion started: 28 July 2026

MATSIRO-GW contribute to larger Q_{subsurf} compared to the original MATSIRO. Interestingly, hydrologic models, for example, often do not use the concept of f_{sat} (e.g. PCR-GLOBWB (Sutanudjaja et al., 2018), HBV (Bergström, 1995), mHM (Samaniego et al., 2010), VIC (Liang et al., 1994), and HYPE (Lindström et al., 2010), which might be due to the high spatial resolutions they are applied on. It might hence be less required in LSMs in the future to include such subgrid parameterization given that the models will be used on higher spatial resolutions as well.

Soil water limitation of plants

Transpiration E_{trans} gets limited by soil hydraulic properties when soil moisture becomes so low that plants need to exert considerable suction to further extract water from the soil. Soil water retention varies with particle size so that soil texture is an important parameter for water limitation of plants (Liu et al., 2017, 2020; Wankmüller et al., 2024, see Appendix).

E_{trans} was quite similar on sandy and silty soils except in hot dry regions and for NOAH-MP and ORCHIDEE in cold regions. Here, the effects of soil water on transpiration were approximated with stress functions (f_{stress}) that showed qualitatively the same changes between experiments than transpiration. They worked quantitatively only for JSBACH and the MATSIRO models, though, but they were the best possible proxies that could be determined from standard output variables of LS3MIP (van den Hurk et al., 2016). Soil water limitation on plants is not always a simple stress function in land surface models, or the models apply the stress functions on different parts of the model such as on stomatal conductance, on biochemical reaction rates, or both (Egea et al., 2011). Wankmüller et al. (2024) defined the onset of water limitation as the point when the sensitivity of transpiration to leaf water potential reached 80% of its maximum. Such detailed analysis is not possible in a model intercomparison project, also because most models did not calculate leaf water potential.

CLM5 and ISBA had the smallest changes of E_{trans} amongst the SP-MIP models when changing from sandy to silty soils. CLM5 was the only model in the SP-MIP ensemble that included plant hydraulics, i.e. regulates root water uptake and transpiration via water potentials within the plants (Kennedy et al., 2019). The plants can adjust their water potentials so that water supply suffices demand, and they can hence take up water from deeper soil layers if the topsoil dries out. A large number of land surface models are currently implementing plant hydraulics (e.g. De Kauwe et al., 2020; Yao et al., 2022) so that such compensation effects will be more prominent in models in the future.

ISBA shows generally very little response to soil droughts (Bastos et al., 2020). Δf_{stress} exaggerated ΔE_{trans} for ISBA during summer in our case because the soil water stress in ISBA limits first independently mesophyll conductance or the model sensitivity to vapour pressure deficit, depending on plant type (tall or short, drought avoiding or drought tolerant), before it secondly limits both simultaneously (Calvet et al., 2004). Our proxy for the stress function behaved thus qualitatively similar to transpiration in ISBA but was quantitatively much too strong. Our results, however, confirmed the results of Bastos et al. (2020) that soil moisture plays a limited role for plant transpiration in ISBA.

The proxies for soil water stress worked quantitatively only for three out of the seven SP-MIP models. Other models would need to change their source code extensively to really assess soil water limitations. It will become even more difficult once LSMs include full descriptions of plant hydraulics (Kennedy et al., 2019) or implement new schemes of "stomatal optimization" (Sabot et al., 2022). One could try to base the analysis on, for example, evaporative fraction ($\lambda E/(\lambda E{+}H)$ with latent heat λE

https://doi.org/10.5194/egusphere-2026-4223
Preprint. Discussion started: 28 July 2026

and sensible heat H), which is used to determine the onset of soil water limitation on evapotranspiration (Fu et al., 2022a, b; Wankmüller et al., 2024). However, more work needs to be done to turn the evaporative fraction into a quantitative measure of soil water limitation.

5 Conclusions

The land surface models (LSM) that participated in SP-MIP were structurally quite similar in terms of their simulations of water fluxes. They conceptualized water fluxes in similar terms such as surface runoff (Q_{surf}) and subsurface runoff (Q_{subsurf}), and all used the Richards equation for soil water movement, although in different functional forms. They responded strongly to changes from silt to sand parameters imposed in the SP-MIP experiments. The responses were model-specific and very different between the LSMs. They even showed sometimes counter-intuitive results due to model-specific process parameterizations.

Model intercomparisons often identify general patterns of similarity or dissimilarity between models, or benchmark models against observations (e.g. Haughton et al., 2016; Ménard et al., 2021). They rarely point to specific issues within individual models. We demonstrated here that process descriptions like surface runoff and soil evaporation dominate LSM sensitivities for the partitioning of water fluxes. Therefore, the top layer of land surface models can be perceived as a super-critical zone, where improved process descriptions are truly needed. We do not recommend specific descriptions because they will depend on the overall model structure and the coupling to the atmosphere, amongst other aspects. Our results can, however, help users interpret results of land surface models and can help modelling groups move forward and improve the representation of the water cycle in LSMs.

Code and data availability. Soil texture and parameter maps used in SP-MIP are archived on Zenodo under DOI 10.5281/zenodo.21469535 (Gudmundsson and Cuntz, 2017). Overall mean and dry season mean model outputs together with the scripts to reproduce the Figures and Tables of this manuscript are archived on Zenodo under DOI 10.5281/zenodo.21473084 (Cuntz et al., 2026).

Appendix A

We provide summaries of the descriptions of surface runoff, soil evaporation, and soil water limitation on transpiration in the SP-MIP land surface models. We cannot reproduce the process descriptions in minute detail here, but we present the ideas behind the descriptions. For the detailed process implementations, we refer to the publications or the detailed model descriptions of the modelling centres.

A1 Descriptions of surface runoff in the land surface models

All but two models (NOAH-MP and ORCHIDEE) in SP-MIP used a fractional saturated area f_{sat} in their description of surface runoff, which is based on TOPMODEL (Beven and Kirkby, 1979). This fractional saturated area represents sub-grid variability

https://doi.org/10.5194/egusphere-2026-4223
Preprint. Discussion started: 28 July 2026

of soil properties, topography, and similar and depends on the current soil water status of the grid cell. The actual formulations of f_{sat} differed in the five models.

The part of liquid water that reaches the surface through rain, canopy throughfall, and snow melt ($Q_{\text{liq},0}$) and that falls on the saturated surface ($f_{\text{sat}}Q_{\text{liq},0}$) gives saturation-excess runoff (Dunne runoff). Water infiltrates only in the unsaturated part of the grid cell, i.e. $1-f_{\text{sat}}$. Any excess water in that part leads to infiltration-excess runoff (Horton runoff). Hence, surface runoff depends always on soil water content or water table depth due to saturation-excess runoff. Infiltration into the non-saturated surface depends in the models either on soil water content and/or on hydraulic conductivity.

Here, all water fluxes Q are in $\mathrm{kg\,m^{-2}\,s^{-1}}$, volumetric soil moisture θ is in $\mathrm{m^3\,m^{-3}}$, depth z is in m, hydraulic conductivity k is in $\mathrm{m\,s^{-1}}$, soil water potential or water head ψ is in m, and fractions f are dimensionless.

CLM5

CLM5 uses the runoff model of Niu et al. (2005). The fractional saturated area is:

$$f_{\text{sat}} = f_{\text{sat,max}} \exp(-0.5 f_{\text{z}} z_{\text{wt}}), \tag{A1}$$

where $f_{\text{sat,max}}$ is the maximal possible fractional area to be saturated, f_{z} ($\mathrm{m^{-1}}$) is a reduction factor of hydraulic conductivity with soil depth, and z_{wt} is the water table depth of the grid cell, which is determined by interpolating between the depth of the shallowest saturated soil layer and the depth of the layer above that.

The moisture input at the grid cell surface, $Q_{\text{liq},0}$, is the sum of liquid precipitation reaching the ground and melt water from snow. All water falling on the saturated land surface ($f_{\text{sat}}Q_{\text{liq},0}$) gives surface runoff:

$$Q_{\text{over}} = f_{\text{sat}} Q_{\text{liq},0}. \tag{A2}$$

Another fraction of the grid cell f_{h2osfc} is the fraction of the area that is inundated in CLM5 to represent wetlands and small, sub-grid scale water bodies. If the water storage at the surface exceeds a threshold, then it acts as a linear reservoir:

$$Q_{\text{sfc}} = k_{\text{sfc}} f_{\text{interconnected}} (W_{\text{sfc}} - W_{\text{c}}) \frac{1}{\Delta t}, \tag{A3}$$

where k_{sfc} is a constant, $f_{\text{interconnected}}$ is the fraction of the inundated portion that is interconnected, W_{sfc} is the water stored in inundated areas, and W_{c} is the threshold at which outflow from inundated areas exists. The input to the inundated water storage is all water falling on this portion of the grid cell plus any infiltration excess water, which happens in the unsaturated part of the grid cell. Q_{sfc} and Q_{over} add up to give surface runoff Q_{surf}.

ISBA

ISBA uses a “corrected” TOPMODEL approach (Saulnier and Datin, 2004) where the fractional saturated area is inversely proportional to the mean water storage deficit, D_{t} (m):

$$f_{\text{sat}}^{-1} \propto D_{\text{t}} = (\theta_{\text{sat}} - \theta_{\text{root}}) z_{\text{root}}, \tag{A4}$$

https://doi.org/10.5194/egusphere-2026-4223
Preprint. Discussion started: 28 July 2026

where θ_{root} and z_{root} are the mean volumetric soil moisture and depth of the root zone, respectively, weighted by the relative fraction of each land surface tile of a grid cell (Decharme and Douville, 2006). θ_{root} must also be greater than the wilting point.

ISBA assumes sub-grid variability in local rainfall that follows an exponential probability distribution. Local sub-grid infiltration (using superscript i) in unfrozen soil is given by:

$$Q^i_{\text{infl,unfrozen}} = k^i_{\text{sat}} \left[\frac{b\psi_{\text{sat}}}{\Delta z} \left(\frac{\theta^i_{\text{root}}}{\theta^*_{\text{sat}}} - 1 \right) + 1 \right], \tag{A5}$$

with k^i_{sat} the local sub-grid saturated hydraulic conductivity, ψ_{sat} is the saturated soil water potential or air entry potential, Δz is a soil thickness of 0.1 m, b is the pore size distribution index from the Brooks–Corey equation, θ^i_{root} is the local sub-grid mean volumetric soil moisture of the root zone, and θ^*_{sat} is the saturated soil porosity when soil ice is present. Any liquid water reaching the non-saturated, unfrozen surface that cannot infiltrate gives infiltration excess runoff. It adds to saturation excess runoff as well as any water that falls on frozen ground (Decharme et al., 2019); the latter becoming runoff immediately.

JSBACH

Hagemann and Stacke (2015) extended the original Arno scheme (Dümenil and Todini, 1992) to a new five layer soil hydrology scheme. However, fractional saturated area and infiltration remained unchanged. It uses root-zone soil moisture θ_{root} to calculate f_{sat} (Modellbetreuungsgruppe, 1994):

$$f_{\text{sat}} = 1 - \left(1 - \frac{\theta_{\text{root}}}{\theta_{\text{sat}}} \right)^b, \tag{A6}$$

where the structure parameter b is parameterized with the standard deviation of the terrain height of the respective grid cell.

Saturation-excess runoff is produced if precipitation (or snow melt) yields oversaturation, i.e. $(\theta_{\text{root}} z_{\text{root}} + Q_{\text{liq,0}}) > \theta_{\text{sat}} z_{\text{root}}$, with z_{root} the depth of the root zone. Surface runoff is then the well-known "bucket model":

$$Q_{\text{surf}} = Q_{\text{liq,0}} - (\theta_{\text{sat}} - \theta_{\text{root}}) z_{\text{root}}. \tag{A7}$$

If precipitation is not yielding oversaturation, surface runoff is modified to:

$$\begin{aligned} Q_{\text{surf}} = {} & Q_{\text{liq,0}} - (\theta_{\text{sat}} - \theta_{\text{root}}) z_{\text{root}} \\ & + \theta_{\text{sat}} z_{\text{root}} \left[\left(1 - \frac{\theta_{\text{root}}}{\theta_{\text{sat}}} \right)^{\frac{1}{1+b}} - \frac{Q_{\text{liq,0}}}{(1-b)\theta_{\text{sat}} z_{\text{root}}} \right]^{1+b}. \end{aligned} \tag{A8}$$

See Reick et al. (2021) for a detailed derivation of this expression.

MATSIRO, MATSIRO-GW

The MATSIRO model family also uses a simplified TOPMODEL-approach for runoff (Takata et al., 2003). The fractional saturated area is calculated as:

$$f_{\text{sat}} = 1 - \exp(f_z z_{\text{wt}} - 1), \tag{A9}$$

https://doi.org/10.5194/egusphere-2026-4223
Preprint. Discussion started: 28 July 2026

where f_z is a reduction factor of hydraulic conductivity with soil depth (m^{-1}) and z_{wt} is the mean water table depth of the grid cell. The latter changed substantially when a groundwater reservoir was introduced in MATSIRO (Koirala et al., 2014).

Maximum infiltration into unsaturated soil is the saturated conductivity of the first soil layer, $k_{\mathrm{sat},1}$. Actual infiltration is input water to the soil with infiltration-excess runoff subtracted:

$$Q_{\mathrm{surf}} = Q_{\mathrm{liq,0}} - (1 - f_{\mathrm{sat}})\max(Q_{\mathrm{liq,0}} - k_{\mathrm{sat},1}, 0). \quad \text{(A10)}$$

NOAH-MP

NOAH-MP is based on the original NOAH model (Chen and Dudhia, 2001), introducing multiple options for all processes (MP) represented in NOAH (Niu et al., 2011). For SP-MIP, the original formulation of NOAH for runoff and infiltration (option 3) was chosen (Schaake et al., 1996). It assumes an exponential distribution of infiltration capacities, $Q_{\mathrm{infl,capacity}}$, within each grid cell, so that the actual spatially-averaged infiltration in the grid cell is:

$$Q_{\mathrm{infl}} = \frac{Q_{\mathrm{liq,0}} Q_{\mathrm{infl,capacity}}}{Q_{\mathrm{liq,0}} + Q_{\mathrm{infl,capacity}}}. \quad \text{(A11)}$$

Starting from the fact that infiltration can be correlated with soil moisture deficit, NOAH(-MP) assumes that infiltration will fill up the soil moisture deficit after long times (days to months) but it is less than the soil moisture deficit for shorter time scales:

$$Q_{\mathrm{infl,capacity}} = (\theta_{\mathrm{sat}} - \theta_{\mathrm{root}}) z_{\mathrm{root}} \left[1 - \exp(-K_{\mathrm{dt}} \Delta t)\right], \quad \text{(A12)}$$

where θ_{root} and z_{root} are the mean volumetric soil moisture and the depth of the root zone, respectively. The soil moisture deficit is ($\theta_{\mathrm{sat}} - \theta_{\mathrm{root}}$) z_{root} here. K_{dt} is a time constant (day^{-1}) and Δt is the modelling time step in days. Any water $Q_{\mathrm{liq,0}}$ that is not infiltrated is routed directly to surface runoff Q_{surf}.

ORCHIDEE

In ORCHIDEE, surface runoff generation is based on an infiltration-excess process. The parameterization of infiltration is based on the idea of a wetting front (Heber Green and Ampt, 1911). A time-splitting procedure is used to describe the wetting front propagation during a time step (d'Orgeval et al., 2008). Infiltration is described by iteratively saturating soil layers from top to bottom. The infiltration rate into a specific soil layer j is taken as the arithmetic mean of the actual hydraulic conductivity of this layer, k_j, and the saturated hydraulic conductivity of the soil layer just above, $k_{\mathrm{sat},j-1}$, which was just being saturated before:

$$Q_{\mathrm{infl},j} = (k_j + k_{\mathrm{sat},j-1})/2. \quad \text{(A13)}$$

Like ISBA, ORCHIDEE also assumes a subgrid-variability based on an exponential probability distribution, but applied on the saturated hydraulic conductivity. Infiltration-excess runoff is produced where $Q_{\mathrm{liq,0}}$ is larger than the local infiltration rate

https://doi.org/10.5194/egusphere-2026-4223
Preprint. Discussion started: 28 July 2026

defined by the exponential distribution. Spatial integration leads to a reduced infiltration rate in each soil layer compared to the uniform case of equation A13:

$$Q^*_{\text{infl},j} = Q_{\text{infl},j}\left[1 - \exp(-Q_{\text{liq},0}/Q_{\text{infl},j})\right]. \tag{A14}$$

The part of $Q_{\text{liq},0}$ that has not infiltrated in a soil layer at the end of the time step defines the potential surface runoff, which will only run off effectively if the slope is large enough. To this end, ORCHIDEE uses a ponding fraction, f_{pond}, defining the fraction of potential surface runoff that is allowed to pond locally and infiltrate at the next time step:

$$f_{\text{pond}} = 1 - \min(1, S/S_{\text{max}}), \tag{A15}$$

where S is the mean slope in the grid cell and S_{max} is the slope threshold above which no ponding occurs, taken here as 0.5%. The ponded runoff will be added at the next time step to the liquid water reaching the surface, $Q_{\text{liq},0}$, while the rest defines the effective surface runoff, Q_{surf}.

A2 Descriptions of soil evaporation in the land surface models

Soil evaporation E_{soil} is parameterized as:

$$E_{\text{soil}} = \rho_{\text{air}}\beta(\alpha q_{\text{sat}} - q_{\text{air}}), \tag{A16}$$

where ρ_{air} is air density ($\text{kg}\,\text{m}^{-3}$), β the exchange coefficient, α relative humidity at the evaporating front in the soil, q_{sat} the saturation specific humidity at the soil temperature at the evaporating front ($\text{kg}\,\text{kg}^{-1}$), and q_{air} the specific humidity of the air at a reference height.

The exchange coefficient β is:

$$\beta = \frac{1}{r_{\text{aw}} + r_{\text{soil}}}, \tag{A17}$$

with r_{aw} the aerodynamic resistance to water vapour transfer between the soil surface and the reference height ($\text{s}\,\text{m}^{-1}$) and r_{soil} the resistance to water vapour transfer from the evaporating front to the soil surface. The aerodynamic resistance r_{aw} is often related to windspeed u ($\text{m}\,\text{s}^{-1}$) by $r_{\text{aw}}^{-1} = C_{\text{H}}u$ with the drag coefficient C_{H}, especially over bare soil.

The land surface models differ mostly in how they interpret α, for example as the relative humidity within the soil or the relative humidity at the soil surface, and if they include a soil resistance r_{soil} and how it is parameterized.

In addition to the nomenclature of the section before, resistance r, the inverse conductance k^{-1}, is in $\text{s}\,\text{m}^{-1}$ and specific humidity q is in $\text{kg}\,\text{kg}^{-1}$.

CLM5

CLM5 uses soil moisture potential and temperature of the first soil layer ($2\,\text{cm}$) to calculate soil relative humidity (Lawrence et al., 2018) using the Kelvin equation (Philip, 1957):

$$\alpha = \exp\left(\frac{M_{\text{w}}\psi_{\text{s},1}g}{RT_{\text{s},1}}\right), \tag{A18}$$

https://doi.org/10.5194/egusphere-2026-4223
Preprint. Discussion started: 28 July 2026

with M_w the molar mass of water ($\mathrm{kg\,mol^{-1}}$), $\psi_{\mathrm{s},1}$ the pressure head of the first soil layer (m), g the gravity of Earth ($\mathrm{m\,s^{-2}}$), R the molar gas constant ($\mathrm{l\,mol^{-1}\,K^{-1}}$), and $T_{\mathrm{s},1}$ the soil temperature of the first soil layer (K).

Soil resistance of equation A17 is calculated as a resistance due to molecular diffusion through a dry soil layer:

$$r_\mathrm{soil} = \frac{L}{D\tau}, \tag{A19}$$

with the dry layer thickness L (m), D the molecular diffusivity of water vapour in air ($\mathrm{m^2\,s^{-1}}$), and τ the tortuosity of the vapour flow path through the soil matrix (Moldrup et al., 2003). The dry layer thickness is parameterized as a function of the soil moisture of the first soil layer, θ_1:

$$L = \begin{cases} \Delta z_\mathrm{L} \frac{\theta_\mathrm{L0} - \theta_1}{\theta_\mathrm{L0} - \theta_\mathrm{air}} & \theta_1 < \theta_\mathrm{L0} \\ 0 & \theta_1 \geq \theta_\mathrm{L0} \end{cases} \tag{A20}$$

with Δz_L a parameter specifying the length scale of the maximum thickness of L (m), θ_air the "air-dry" soil moisture defined at a matric potential of 10^4 m, and θ_L0 the moisture value at which the dry surface layer initiates. Δz_L is taken as 15 mm and θ_L0 is taken as a constant fraction (0.8) of soil porosity (Swenson and Lawrence, 2014).

The specific humidity of the air q_air in equation A16 is the surface specific humidity at the scalar roughness lengths for sensible heat z_0h plus displacement height d, i.e. $z_\mathrm{0h} + d$.

ISBA

ISBA was run with the multi-energy balance option (Boone et al., 2017, ISBA-MEB,), which then gives a hybrid approach for soil evaporation, that means it uses r_soil = 0 for bare soil evaporation and a parameterization of r_soil for soil evaporation below vegetation, where aerodynamic resistance r_aw is also greatly reduced compared to the bare soil fraction.

ISBA uses the surface ground humidity factor of Noilhan and Planton (1989) for α:

$$\alpha = \frac{1}{2}\left[1 - \cos\left(\frac{\theta_1}{\theta_{\mathrm{fc},1}}\pi\right)\right] \; (0 \leq \alpha \leq 1), \tag{A21}$$

with $\theta_{\mathrm{fc},1}$ the field capacity (adjusted in the presence of soil ice) of the uppermost soil layer.

Soil resistance is calculated after Sellers et al. (1992):

$$r_\mathrm{soil} = \exp\left[a_\mathrm{I} - b_\mathrm{I}(\overline{\theta}/\overline{\theta}_\mathrm{sat})\right], \tag{A22}$$

with the coefficients a_I = 8.206 and b_I = 4.255. The volumetric water content and saturated volumetric water contents are averaged over one to several upper soil layers. Both, α and r_soil are adjusted when soil ice is present.

The specific humidity of the air q_air in equation A16 is the specific humidity of a canopy air space, equivalent to the surface specific humidity of CLM5.

ISBA has now also an option to use the same formulation of soil evaporation as CLM5 (Martí et al., 2025) but this was not used in the SP-MIP runs yet.

https://doi.org/10.5194/egusphere-2026-4223
Preprint. Discussion started: 28 July 2026

JSBACH

JSBACH is using $r_{\text{soil}} = 0$ for bare soil evaporation, and α is also the surface ground humidity factor of Noilhan and Planton (1989) as in ISBA:

$$\alpha = \max\left\{\frac{1}{2}\left[1-\cos\left(\frac{\theta_1}{\theta_{\text{fc},1}}\pi\right)\right], \min\left\{1, \frac{q_{\text{air}}}{q_{\text{sat}}}\right\}\right\}. \tag{A23}$$

545 The drag or heat transfer coefficient C_{H} depends on surface roughness and atmospheric stability (Giorgetta et al., 2013). Soil evaporation happens only where the surface is not wet or covered by snow or vegetation. Vegetation fraction is thereby a function of leaf area index (LAI) (Reick et al., 2021).

MATSIRO and MATSIRO-GW

The MATSIRO models also use the Kelvin equation (Philip, 1957) to calculate relative humidity in the soil as in CLM5
550 (Eq. A18). Soil resistance of snow- and ice-free surfaces is calculated as (Takata et al., 2003):

$$r_{\text{soil}} = a_1 \frac{1-\theta_1/\theta_{\text{sat}}}{a_2+\theta_1/\theta_{\text{sat}}}, \tag{A24}$$

with the empirical constants $a_1 = 800$ and $a_2 = 0.2$. The formulation of soil resistance is functionally similar to the formulation of Sellers et al. (1992) used in ISBA and ORCHIDEE.

NOAH-MP

555 NOAH-MP is using the same idea as CLM5 of a soil resistance due to molecular diffusion through a dry soil layer but is using the formulation of Sakaguchi and Zeng (2009). They use a different formulation of soil tortuosity by Moldrup et al. (2004) and parameterize the thickness of the dry surface layer as:

$$L = \Delta z_1 \frac{\exp([1-\theta_1/\theta_{\text{sat}}]^w)}{\text{e}-1}, \tag{A25}$$

with Δz_1 the thickness (m) and θ_1 the soil moisture of the first soil layer, e the Euler constant, θ_{sat} saturated soil porosity, and
560 w a parameter that controls the concavity of the curve, which is set to 5. See Swenson and Lawrence (2014) for a comparison between the formulations of CLM5 and of Sakaguchi and Zeng (2009).

ORCHIDEE

ORCHIDEE uses:

$$E_{\text{soil}} = \beta_{\text{s}} E_{\text{pot}}. \tag{A26}$$

565 where potential evaporation (E_{pot}) from the bare soil fraction is calculated with $r_{\text{soil}} = 0$ and $\alpha = 1$, and β_{s} is $E_{\text{soil}}/E_{\text{pot}}$ from the last time step.

https://doi.org/10.5194/egusphere-2026-4223
Preprint. Discussion started: 28 July 2026

To calculate β_s for the next time step, E_{soil} is calculated with a supply-demand approach:

$$E_{soil} = \min\left\{\rho_{air}\frac{q_{sat}(T_w) - q_{air}}{r_{aw} + r_{soil}}, Q_{up}\right\}. \tag{A27}$$

In the demand part, r_{soil} is calculated after Sellers et al. (1992) as in equation A22 of ISBA, with the average volumetric water contents taken over the top four soil layers, which corresponds to a litter zone of about 2.5 cm in the default vertical discretization of ORCHIDEE. $q_{sat}(T_w)$ is the specific humidity of saturated air at the temperature of the (hypothetically wet) evaporating surface. The temperature T_w is found by solving an energy balance equation after Milly (1992). It is generally lower than surface temperature so that the demand is lower than E_{pot} even for r_{soil} = 0.

The supply part solves the Richards equation if it were evaporating with potential evaporation E_{pot}. The soil can supply as much water (Q_{up}) that the top four soil layers do not fall below residual soil moisture if it were evaporating with potential evaporation E_{pot} (Campoy, 2013).

A3 Descriptions of soil water limitation on transpiration in the land surface models

This section summarizes the parameterizations of soil water limitation on transpiration in the different LSMs. There are two groups of models. The first group uses a limitation that is based on soil water potentials (CLM5, MATSIRO, MATSIRO-GW). The second group uses volumetric soil moisture to calculate a limitation term (ISBA, JSBACH, NOAH-MP, and ORCHIDEE). All models calculate a factor that reduces, for example, stomatal conductance, biochemical rates, or evaporation. This is often called a soil water limitation factor or stress factor f_{stress}.

In addition to the nomenclatures of the sections before, θ_{fc} denotes volumetric soil moisture at field capacity and θ_{wp} is the moisture at the permanent wilting point.

CLM5

The description of plant water uptake in CLM5 is described in detail in Kennedy et al. (2019) and briefly summarized here. CLM5 calculates a water stress factor to limit photosynthesis that is applied to the maximum carboxylation rate of well-watered conditions, denoted as $V_{cmax,ww}$. The actual, “water-limited” maximum carboxylation rate is then calculated as:

$$V_{cmax} = f_{stress} V_{cmax,ww}, \tag{A28}$$

with the stress factor f_{stress}.

CLM5 uses a plant hydraulic model that accounts for water potentials across the soil (ψ_{soil}), root (ψ_{root}), plant (ψ_{plant}) continuum. Those are calculated iteratively to find a solution that conserves fluxes over the soil-root-plant-atmosphere system. At the leaf level, the restriction of carboxylation is directly related to the leaf water potential by a logistic equation:

$$f_{stress} = 2^{-(\psi_{leaf}/\psi_{l,50})^{c_k}}, \tag{A29}$$

where ψ_{leaf} is leaf water potential, $\psi_{l,50}$ is the leaf water potential at 50% loss of stomatal conductance, and c_k is a shape parameter. $\psi_{l,50}$ is a plant-specific parameter that can be derived for water flow through stems ($\psi_{stem,50}$) from trait databases such as TRY (Kattge et al., 2011, 2020). A value of up to 0.5 MPa is then added to $\psi_{stem,50}$ to set $\psi_{l,50}$ used in leaves.

https://doi.org/10.5194/egusphere-2026-4223
Preprint. Discussion started: 28 July 2026

Water demand is calculated by using the Medlyn stomatal conductance model that accounts for atmospheric vapour pressure deficit (Medlyn et al., 2011). This model is first run in unstressed conditions and is then limited by applying:

$$E = f_{\text{stress}} E_{\text{max}}, \tag{A30}$$

where f_{stress} is calculated from equation A29. Equation (A30) is applied to both sunlit and shaded leaves.

Root water uptake in soil layer j, $Q_{\text{root},j}$, is calculated based on Darcy's law as:

$$Q_{\text{root},j} = -k_{\text{sr},j}(\psi_{\text{root}} - \psi_{\text{soil},j} + \rho g z_j), \tag{A31}$$

where the soil-root conductivity $k_{\text{sr},j}$ depends root area parameter, ψ_{root} and $\psi_{\text{soil},j}$ are the root and soil water potentials in layer j, respectively, and the last term accounts for gravitational effects. The influence of roots on conductivity is considered in the following way:

$$k_{\text{sr},j} = k_j RAI_j = k_j f_{\text{A,root}}(SAI + LAI) f_{\text{root},j}, \tag{A32}$$

where $f_{\text{A,root}}$ is a relative root area parameter, SAI and LAI are stem and leaf area indexes, respectively, and $f_{\text{root},j}$ is the fraction of roots in the soil layer. k_j are root and soil water conductances in serial, where soil water conductance is calculated per root length.

ISBA

The limitation of transpiration to soil moisture is based on the extractable soil water content in a soil layer:

$$f_j = \frac{\theta_j - \theta_{\text{wp}}}{\theta_{\text{fc}} - \theta_{\text{wp}}}, \tag{A33}$$

with the stress factor:

$$f_{\text{stress}} = \frac{1}{f_{\text{c}}} \sum_{j=1}^{N_{\text{root}}} f_j f_{\text{root},j}, \tag{A34}$$

where $f_{\text{root},j}$ is the root fraction in layer j of N_{root} soil layers with roots, and f_{c} is a critical threshold.

The stress factor is either applied on mesophyll conductance directly or on the sensitivity of mesophyll conductance to vapour pressure. This depends on plant functional type and their drought avoiding or drought tolerating strategies. Full details can be found in Calvet et al. (2004) and Joetzjer et al. (2015).

JSBACH

JSBACH limits transpiration by modifying canopy conductance with a stress factor. The scaling factor represents the relative soil moisture in the root zone, which is calculated as:

$$f_{\text{stress}} = \frac{\theta - \theta_{\text{wp}}}{\theta_{\text{crit}} - \theta_{\text{wp}}}, \tag{A35}$$

https://doi.org/10.5194/egusphere-2026-4223
Preprint. Discussion started: 28 July 2026

limited between 0 and 1.

The critical soil moisture and permanent wilting point are estimated as 75% and 35% of maximum soil moisture, respectively. The stressed canopy conductance is then calculated as:

$$g_{\mathrm{s,stressed}} = \begin{cases} f_{\mathrm{stress}} g_{\mathrm{s}} & \text{for } q_{\mathrm{a}} \leq q_{\mathrm{s}}, \\ 0 & \text{otherwise.} \end{cases} \tag{A36}$$

Stomatal conductance is set to zero if atmospheric specific humidity in the lowest layer, q_{a}, is greater than the saturated value at the surface, q_{s}. The stress factor f_{stress} is applied to stomatal conductance of all canopy layers.

Transpiration (E_{trans}) is extracted from the entire root zone. There is no root distribution with depth. Water extraction from the soil takes place homogeneously down to the rooting depth, but only for soil moisture above the permanent wilting point, $\theta_{\mathrm{wp,veg}}$:

$$E_{\mathrm{trans}}(z) = \begin{cases} \frac{E_{\mathrm{trans}}}{\|z_{\mathrm{root}}\|} & \text{for } z > z_{\mathrm{root}} \text{ and } \theta > \theta_{\mathrm{wp,veg}}, \\ 0 & \text{otherwise.} \end{cases} \tag{A37}$$

If soil water is below or at the wilting point somewhere in the soil, the full amount of E_{trans} cannot be extracted from the soil and E_{trans} reduces accordingly. Note that JSBACH uses two wilting points. One vegetation-specific value that is used in equation A37 and at which plants stop extracting water from the soil and one wilting point at which all soil water movement stops.

MATSIRO and MATSIRO-GW

The LSMs of the MATSIRO family follows the SiB2 model to calculate a soil moisture stress factor in each soil layer relative to unsaturated matric potential (Sellers et al., 1996):

$$f_j = \frac{1}{1 + \exp(0.02(\psi_{\mathrm{crit}} - \psi_j))},$$

where ψ_{crit} is the critical matric potential at which transpiration starts to be reduced, which is a plant-specific parameter. Typical values range between -200 to -300 (Table 5 in Sellers et al., 1996). ψ_j is the soil matric potential calculated as $\psi_{\mathrm{s}}(\theta_j/\theta_{\mathrm{sat}})^{-b}$. These values are then weighted with root fraction to obtain the overall stress factor:

$$f_{\mathrm{stress}} = \sum_{j=1}^{N_{\mathrm{root}}} f_j f_{\mathrm{root},j}, \tag{A38}$$

where $f_{\mathrm{root},j}$ is the root fraction in layer j, which is land cover dependent and has to sum to one over all soil layers. f_{stress} is then used to distribute transpiration to root water uptake in the soil layers:

$$Q_{\mathrm{root},j} = \frac{f_j f_{\mathrm{root},j}}{f_{\mathrm{stress}}} E_{\mathrm{trans}}. \tag{A39}$$

https://doi.org/10.5194/egusphere-2026-4223
Preprint. Discussion started: 28 July 2026

In general, the MATSIRO models calculate photosynthesis using the formulation from the SiB2 model. The reduction factor f_{stress} is used to reduce the carboxylation rate and residual stomatal conductance:

$$V_{\text{cmax}} = V^0_{\text{cmax}} f_{\text{T}} f_{\text{stress}}, \tag{A40}$$

where V^0_{cmax} is the vegetation-specific maximum carboxylation rate and f_{T} and f_{stress} are the temperature and soil water stress factors, respectively. At the same time, the residual conductance b of the Ball-Berry stomatal conductance model (Ball et al., 1987) is reduced as:

$$g_{\text{s}} = m \frac{A_{\text{n}}}{c_{\text{s}}} h_{\text{s}} + b f_{\text{stress}}, \tag{A41}$$

where c_{s} is the molar fraction of CO_2 at the leaf surface, h_{s} relative humidity at the leaf surface, and m and b are vegetation specific parameters.

NOAH-MP

NOAH-MP calculates a soil moisture stress factor that limits the maximum carboxylation rate (Niu et al., 2011). Three options to calculate the stress factor are implemented in NOAH-MP, referred to as β-factors in Niu et al. (2011). These are based on the original NOAH-type implementation, a CLM4-type factor, and a SSIB-type factor (similar to the one used in MATSIRO). Here, the original NOAH-type implementation was used that calculates a linear stress factor f_{stress} between wilting point (full stress) and a reference soil moisture (no stress):

$$f_{\text{stress}} = \sum_{j=1}^{N_{\text{root}}} \frac{\Delta z_j}{z_{\text{root}}} \min(1, \frac{\theta_{\text{liq},j} - \theta_{\text{wp}}}{\theta_{\text{ref}} - \theta_{\text{wp}}}), \tag{A42}$$

where z_{root} is the rooting depth, N_{root} is the number of soil layers within the root zone, and Δz_j is the soil layer thickness of soil layer j. Note that the reference soil moisture value is close to field capacity. Note also that there is no dependency on root distribution in this formulation and lower soil layers receive a higher weight in Equation (A42) due to its larger thickness. However, N_{root} is vegetation-type specific. The stress factor β is then used to limit V_{cmax}:

$$V_{\text{cmax}} = V_{\text{cmax,25}} Q_{10}^{\frac{T_{\text{v}}-25}{10}} f(N) f(T_{\text{v}}) f_{\text{stress}}, \tag{A43}$$

where $V_{\text{cmax,25}}$ is the maximum carboxylation rate at 25 °C, Q_{10} is the temperature sensitivity, $f(N)$ and $f(T_{\text{v}})$ are foliage nitrogen and temperature stress factors, respectively.

ORCHIDEE

Similarly to ISBA, the soil moisture stress factor in ORCHIDEE is defined in each soil layer based on wilting point and a critical soil moisture value:

$$f_j = \frac{\theta_j - \theta_{\text{wp}}}{\theta_{\text{crit}} - \theta_{\text{wp}}}, \tag{A44}$$

https://doi.org/10.5194/egusphere-2026-4223
Preprint. Discussion started: 28 July 2026

limited between 0 and 1. θ_j is soil moisture in layer j and θ_{crit} is a critical soil moisture. The latter is calculated as:

$$\theta_{\text{crit}} = \theta_{\text{wp}} + \alpha(\theta_{\text{fc}} - \theta_{\text{wp}}), \tag{A45}$$

where α is set to 0.8.

The effective soil moisture limitation factor is then calculated as a weighted average of layer-specific factors (Eq. A44) weighted by root fraction:

$$f_{\text{stress}} = \sum_{j=1}^{N_{\text{root}}} f_{\text{root},j} f_j, \tag{A46}$$

where $f_{\text{root},j}$ is the relative root density in soil layer j. The stress factor can be applied either to the maximum carboxylation rate V_{cmax}, to stomatal conductance g_{s}, or to both (MacBean et al., 2020), which results in any case in a limitation of transpiration E_{trans}. The limitation factors f_{stress} and f_j are then used to calculate root water uptake $Q_{\text{root,j}}$ in soil layer j as:

$$Q_{\text{root},j} = \frac{f_j}{f_{\text{stress}}} E_{\text{trans}}. \tag{A47}$$

https://doi.org/10.5194/egusphere-2026-4223
Preprint. Discussion started: 28 July 2026

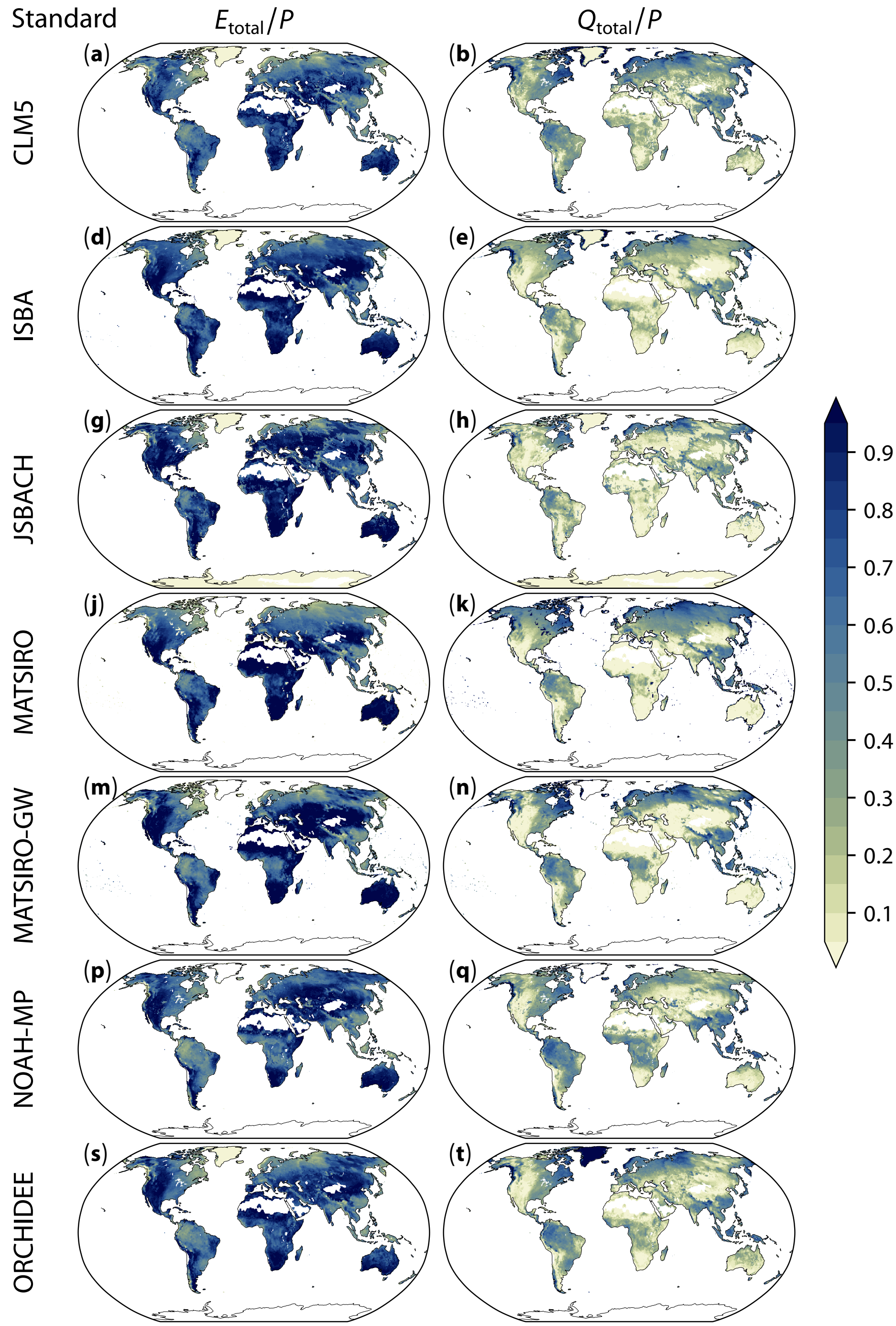

Figure A1. Total evapotranspiration and runoff over precipitation for the model's standard runs. Total evapotranspiration E_{total} (1st column) and total runoff Q_{total} (2nd column) over precipitation. Precipitation water can also be stored in soil and snow. This is temporary in most places so that the mean fluxes over incoming precipitation for 1981-2010 sum up to one at each grid cell for each model (row). Cells with an annual mean precipitation of less than 50 mm were excluded.

https://doi.org/10.5194/egusphere-2026-4223
Preprint. Discussion started: 28 July 2026

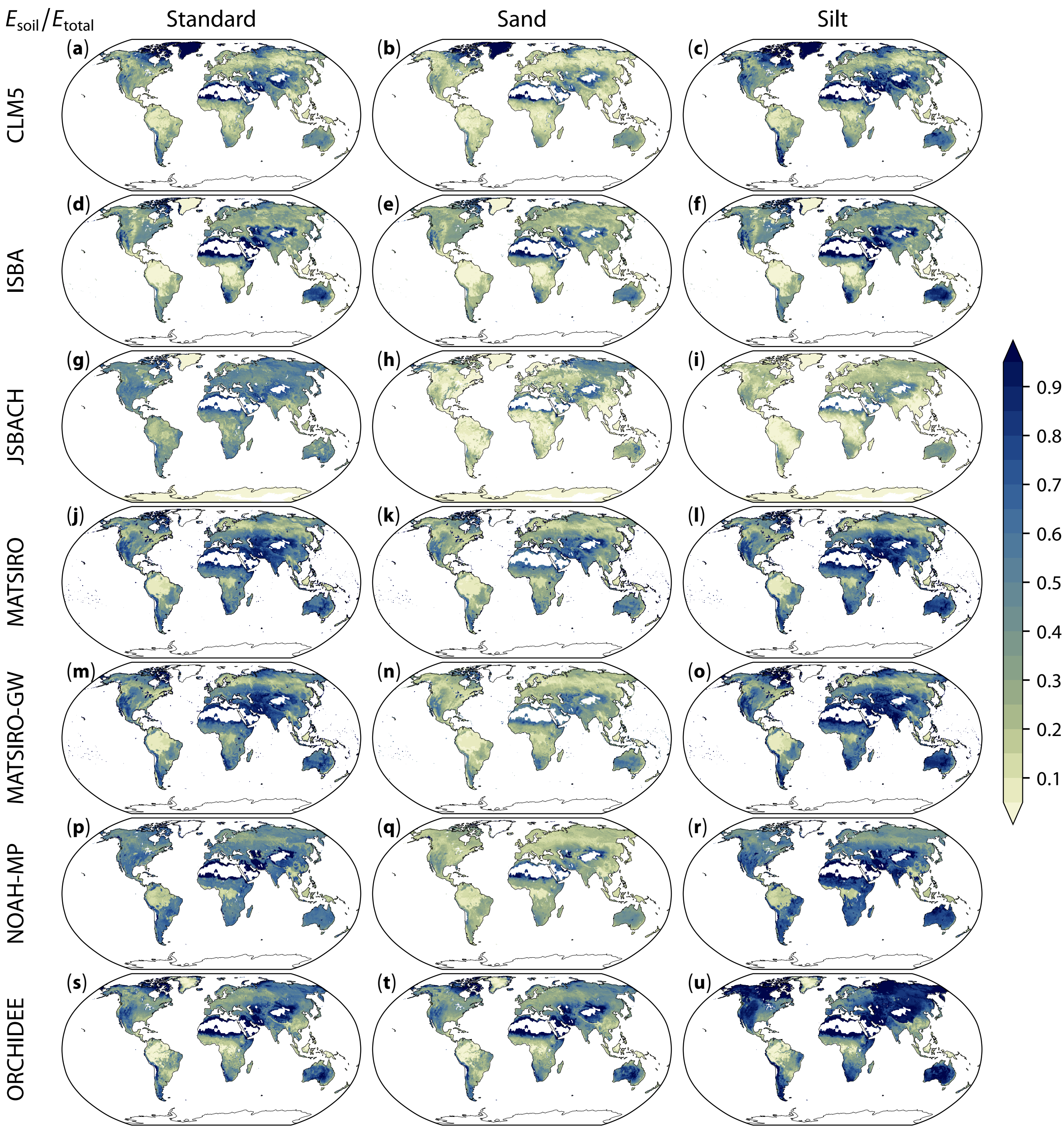

Figure A2. Fraction of soil evaporation. Soil evaporation E_{soil} over total evapotranspiration E_{total} for 1981-2010 for the standard runs (1st column), the sand experiment (2nd column), and the silt experiment (3rd column) for each model (row).

https://doi.org/10.5194/egusphere-2026-4223
Preprint. Discussion started: 28 July 2026

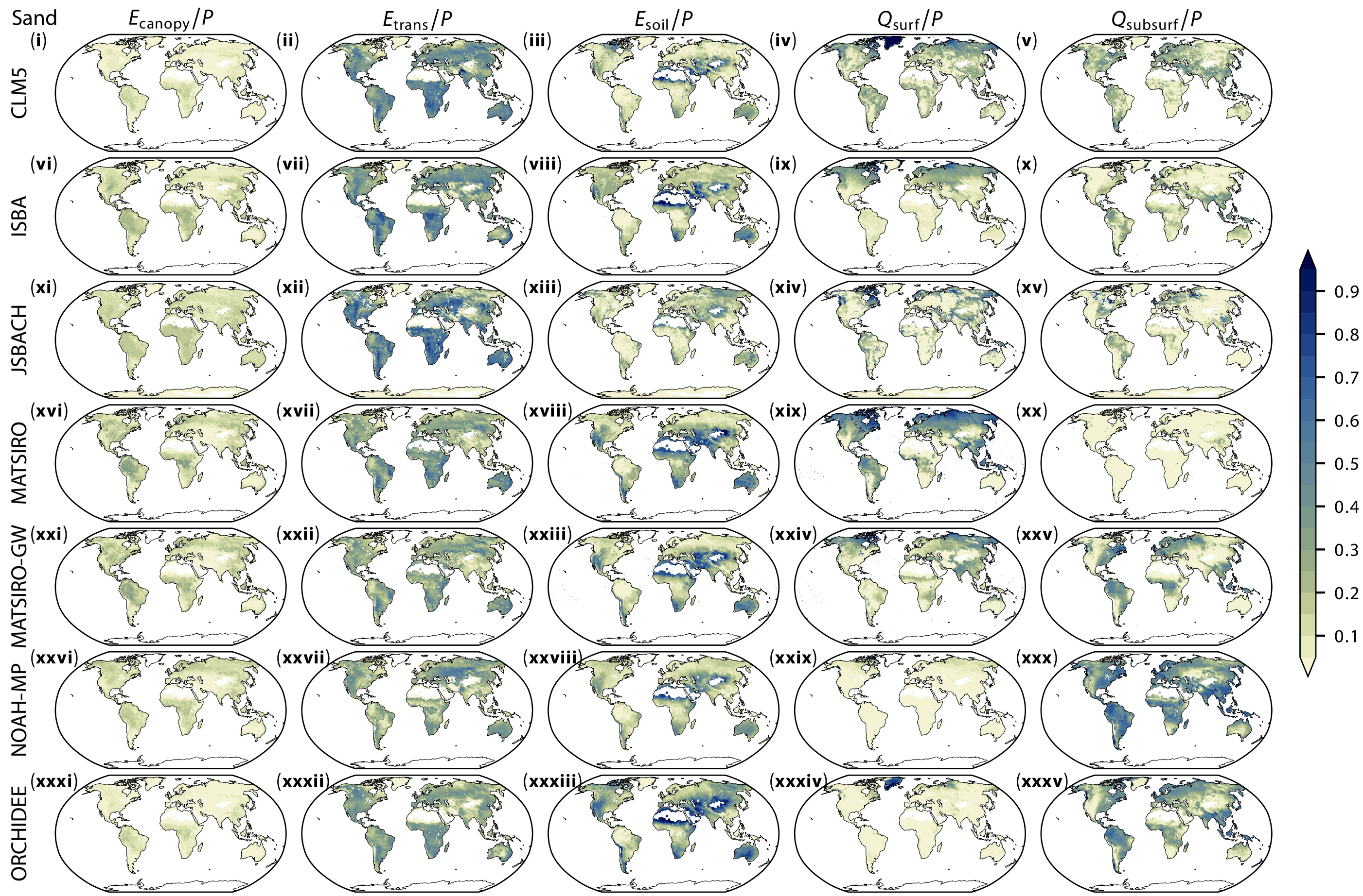

Figure A3. Individual water fluxes at the land surface over precipitation for sandy soil. Same as Figure 2 of the main text but for the sand experiment. Precipitation is partitioned into interception with consequent canopy evaporation E_{canopy} (1st column), transpiration E_{trans} (2nd column), soil evaporation E_{soil} (3rd column), surface runoff Q_{surf} (4th column), and subsurface runoff Q_{subsurf} (5th column). Precipitation water can also be stored in soil and snow. This is temporary in most places so that the mean fluxes over incoming precipitation for 1981-2010 sum up to one at each grid cell for each model (row). Cells with an annual mean precipitation of less than 50 mm were excluded.

https://doi.org/10.5194/egusphere-2026-4223
Preprint. Discussion started: 28 July 2026

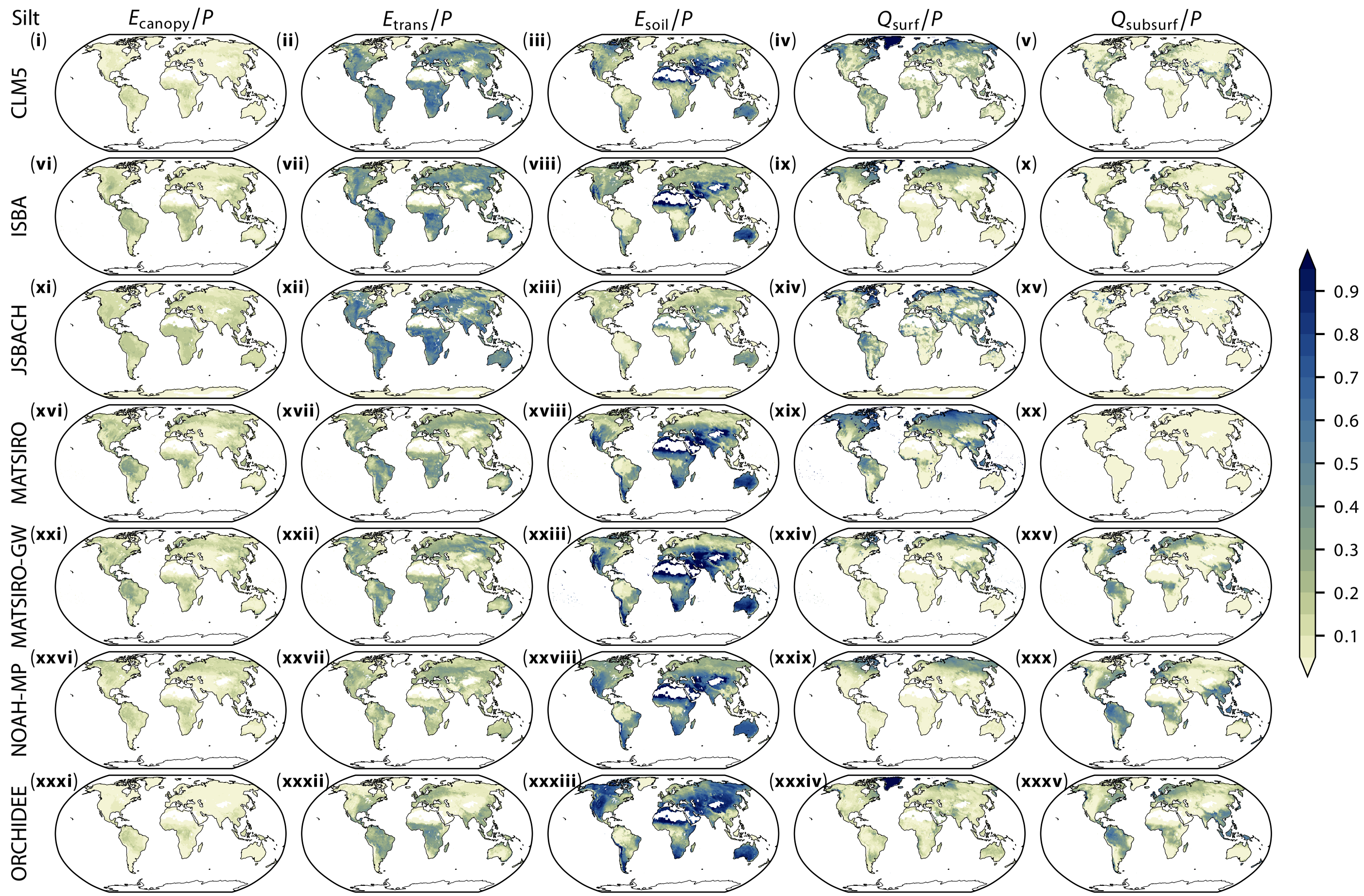

Figure A4. Individual water fluxes at the land surface over precipitation for silty soil. Same as Figure 2 of the main text but for the silt experiment. Precipitation is partitioned into interception with consequent canopy evaporation E_{canopy} (1[st] column), transpiration E_{trans} (2[nd] column), soil evaporation E_{soil} (3[rd] column), surface runoff Q_{surf} (4[th] column), and subsurface runoff Q_{subsurf} (5[th] column). Precipitation water can also be stored in soil and snow. This is temporary in most places so that the mean fluxes over incoming precipitation for 1981-2010 sum up to one at each grid cell for each model (row). Cells with an annual mean precipitation of less than 50 mm were excluded.

https://doi.org/10.5194/egusphere-2026-4223
Preprint. Discussion started: 28 July 2026

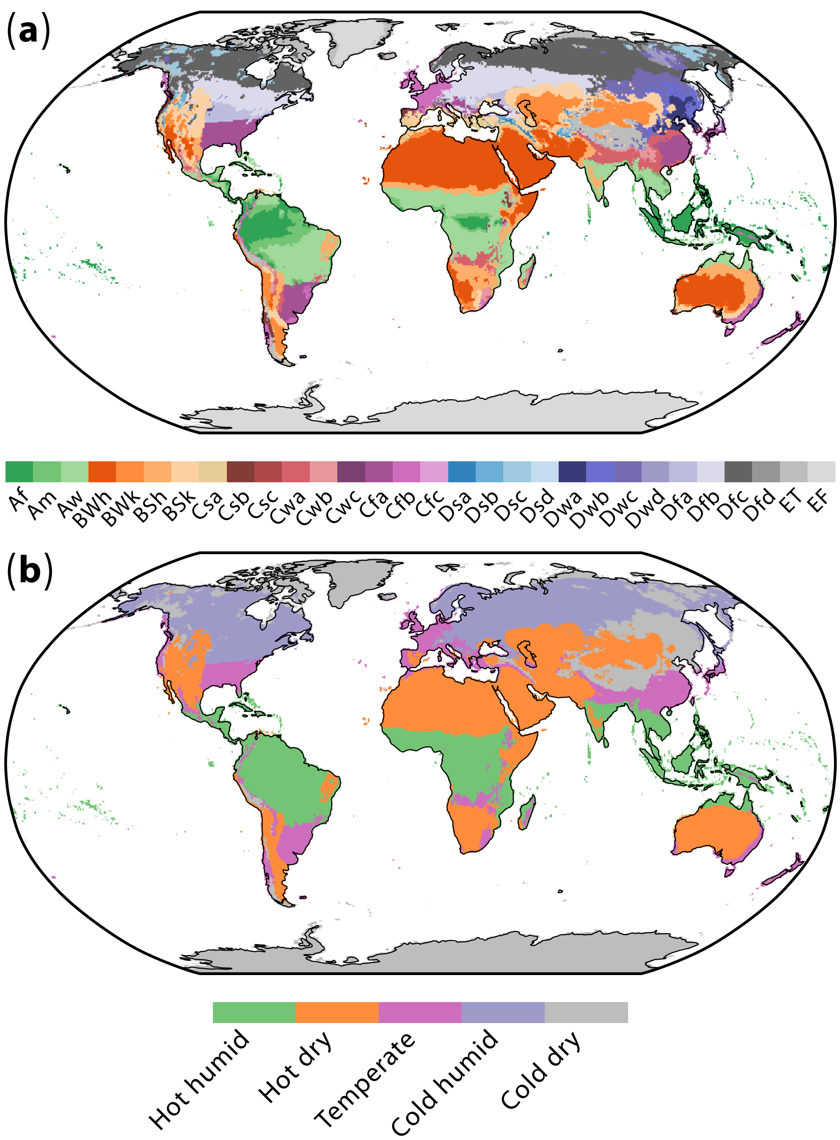

Figure A5. Climate regions. Map of Köppen-Geiger climate regions for 1991–2020 (Beck et al., 2023) (**a**) and the aggregated regions of SP-MIP (**b**). Abbreviations: LSS, leaf soluble sugar concentration; Af, Tropical, rainforest; Am, Tropical, monsoon; Aw, Tropical, savannah; BWh, Arid, desert, hot; BWk, Arid, desert, cold; BSh, Arid, steppe, hot; BSk, Arid, steppe, cold; Csa, Temperate, dry summer, hot summer; Csb, Temperate, dry summer, warm summer; Csc, Temperate, dry summer, cold summer; Cwa, Temperate, dry winter, hot summer; Cwb, Temperate, dry winter, warm summer; Cwc, Temperate, dry winter, cold summer; Cfa, Temperate, no dry season, hot summer; Cfb, Temperate, no dry season, warm summer; Cfc, Temperate, no dry season, cold summer; Dsa, Cold, dry summer, hot summer; Dsb, Cold, dry summer, warm summer; Dsc, Cold, dry summer, cold summer; Dsd, Cold, dry summer, very cold winter; Dwa, Cold, dry winter, hot summer; Dwb, Cold, dry winter, warm summer; Dwc, Cold, dry winter, cold summer; Dwd, Cold, dry winter, very cold winter; Dfa, Cold, no dry season, hot summer; Dfb, Cold, no dry season, warm summer; Dfc, Cold, no dry season, cold summer; Dfd, Cold, no dry season, very cold winter; ET, Polar, tundra; EF, Polar, frost.

https://doi.org/10.5194/egusphere-2026-4223
Preprint. Discussion started: 28 July 2026

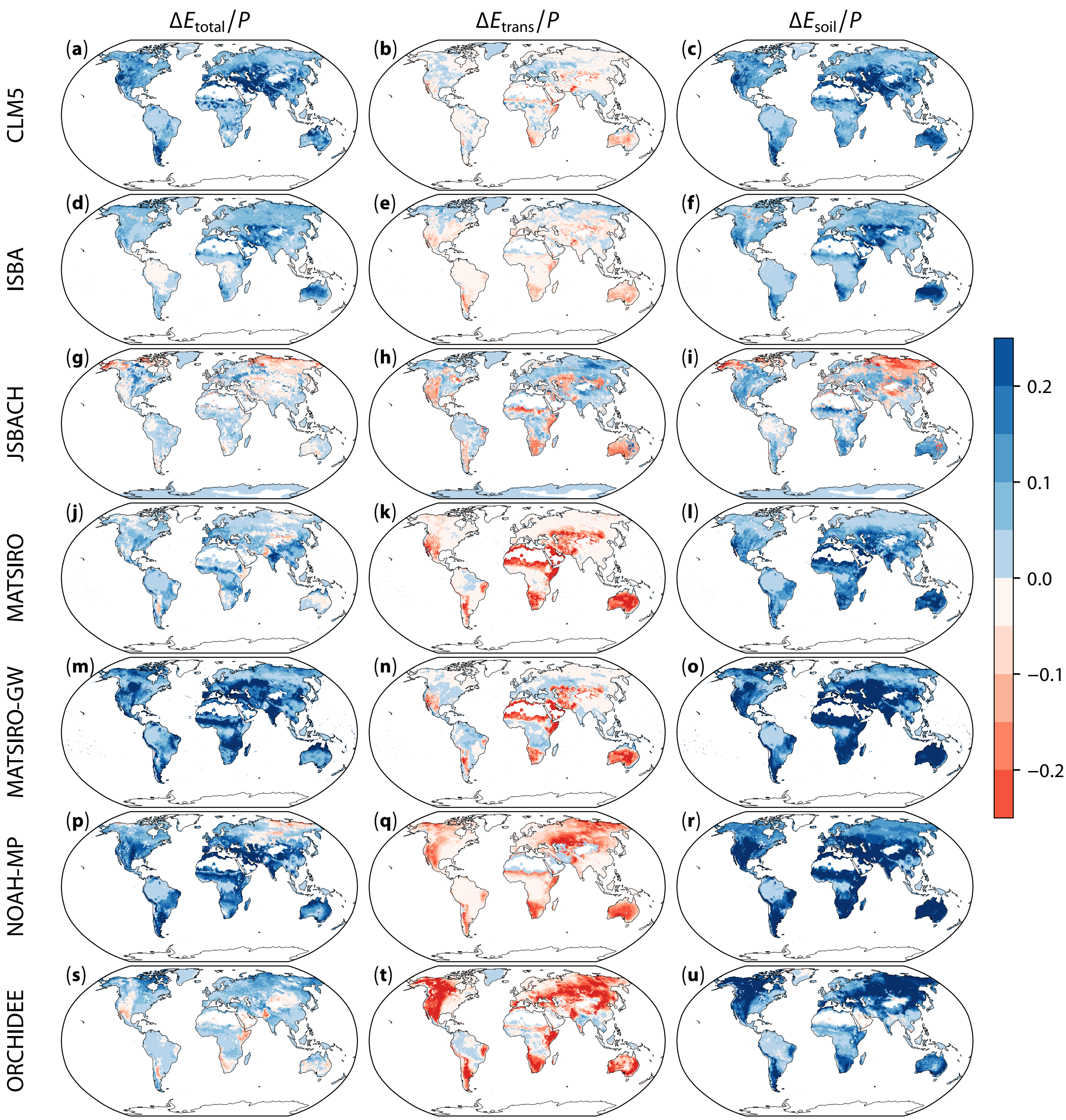

Figure A6. Differences of individual water fluxes over precipitation between the silt and sand experiments. Difference (Δ) of mean evapotranspiration E_{total} over incoming precipitation P for 1981-2010 of the experiment silt minus the experiment sand (1st column) for each model (row), difference of mean soil evaporation E_{soil} over P (2nd column), and difference of surface runoff Q_{surf} over P (3rd column). Cells with an annual mean precipitation of less than 50 mm were excluded.

https://doi.org/10.5194/egusphere-2026-4223
Preprint. Discussion started: 28 July 2026

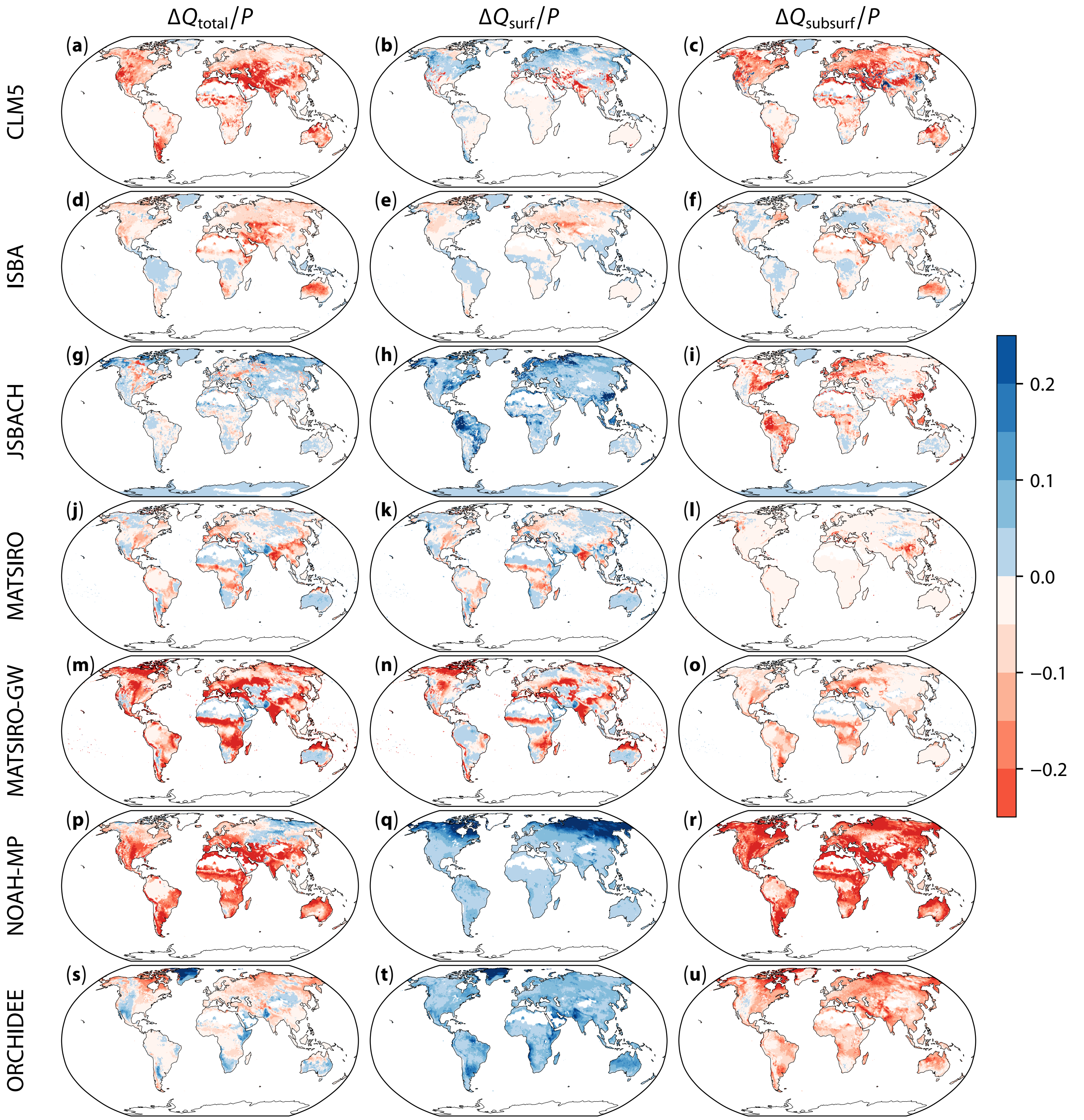

Figure A7. Differences of individual water fluxes over precipitation between the silt and sand experiments. Difference (Δ) of mean total runoff Q_{total} over incoming precipitation P for 1981-2010 of the experiment silt minus the experiment sand (1st column) for each model (row), difference of mean subsurface runoff Q_{subsurf} over P (2nd column), and difference of transpiration E_{trans} over P (3rd column). Cells with an annual mean precipitation of less than 50 mm were excluded.

https://doi.org/10.5194/egusphere-2026-4223
Preprint. Discussion started: 28 July 2026

Author contributions. M.C. and L.G. designed the SP-MIP experiments, with input from D.O., H.V., A.V., and S.S. C.M. provided the map of dominant soil classes. N.M., A.B., P.d.V., S.K., S.Th., and S.Ta. ran the land surface models. M.C. and S.Th. analysed the data. A.V., L.G., and Y.Z. discussed initial results. M.C. and S.Th. wrote the manuscript. All co-authors discussed and commented on the results and the manuscript. M.C. and S.Th. acquired funding for the project.

690 *Competing interests.* Some authors are members of the editorial board of the journal Geoscientific Model Development.

Acknowledgements. M.C. acknowledges support from a grant of the French National Research Agency (ANR, ANR-21-CE02-0033-01), and a grant overseen by ANR as part of the "Investissements d'Avenir" program (ANR-11-LABX-0002-01, Laboratory of Excellence ARBRE). L.G. acknowledges funding from European Union's Horizon Europe research and innovation programme under grant no. 101137682 (AI4PEX). D.M.L and N.M. thank Keith W. Oleson for help with post-processing CLM5 data.

https://doi.org/10.5194/egusphere-2026-4223
Preprint. Discussion started: 28 July 2026

References

Abramowitz, G., Ukkola, A., Hobeichi, S., Cranko Page, J., Lipson, M., De Kauwe, M. G., Green, S., Brenner, C., Frame, J., Nearing, G., Clark, M., Best, M., Anthoni, P., Arduini, G., Boussetta, S., Caldararu, S., Cho, K., Cuntz, M., Fairbairn, D., Ferguson, C. R., Kim, H., Kim, Y., Knauer, J., Lawrence, D., Luo, X., Malyshev, S., Nitta, T., Ogee, J., Oleson, K., Ottlé, C., Peylin, P., de Rosnay, P., Rumbold, H., Su, B., Vuichard, N., Walker, A. P., Wang-Faivre, X., Wang, Y., and Zeng, Y.: On the Predictability of Turbulent Fluxes from Land: PLUMBER2 MIP Experimental Description and Preliminary Results, Biogeosciences, 21, 5517–5538, https://doi.org/10.5194/bg-21-5517-2024, 2024.

Arora, V. K., Katavouta, A., Williams, R. G., Jones, C. D., Brovkin, V., Friedlingstein, P., Schwinger, J., Bopp, L., Boucher, O., Cadule, P., Chamberlain, M. A., Christian, J. R., Delire, C., Fisher, A. R. A., Hajima, T., Ilyina, T., Joetzjer, E., Kawamiya, M., Koven, C. D., Krasting, J. P., Law, R. M., Lawrence, D. M., Lenton, A., Lindsay, K., Pongratz, J., Raddatz, T., Séférian, R., Tachiiri, K., Tjiputra, J. F., Wiltshire, A., Wu, T., and Ziehn, T.: Carbon-Concentration and Carbon-Climate Feedbacks in CMIP6 Models and Their Comparison to CMIP5 Models, Biogeosciences, 17, 4173–4222, https://doi.org/10.5194/bg-17-4173-2020, 2020.

Ball, J. T., Woodrow, I. E., and Berry, J. A.: A Model Predicting Stomatal Conductance and Its Contribution to the Control of Photosynthesis under Different Environmental Conditions, in: Progress in Photosynthesis Research: Volume 4 Proceedings of the VIIth International Congress on Photosynthesis Providence, Rhode Island, USA, August 10–15, 1986, edited by Biggins, J., pp. 221–224, Springer Netherlands, Dordrecht, ISBN 978-94-017-0519-6, https://doi.org/10.1007/978-94-017-0519-6_48, 1987.

Bastos, A., Ciais, P., Friedlingstein, P., Sitch, S., Pongratz, J., Fan, L., Wigneron, J. P., Weber, U., Reichstein, M., Fu, Z., Anthoni, P., Arneth, A., Haverd, V., Jain, A. K., Joetzjer, E., Knauer, J., Lienert, S., Loughran, T., McGuire, P. C., Tian, H., Viovy, N., and Zaehle, S.: Direct and Seasonal Legacy Effects of the 2018 Heat Wave and Drought on European Ecosystem Productivity, Science Advances, 6, https://doi.org/10.1126/sciadv.aba2724, 2020.

Batjes, N.: Harmonized Soil Property Values for Broad-Scale Modelling (WISE30sec) with Estimates of Global Soil Carbon Stocks, Geoderma, 269, 61–68, https://doi.org/10.1016/j.geoderma.2016.01.034, 2016.

Beck, H. E., McVicar, T. R., Vergopolan, N., Berg, A., Lutsko, N. J., Dufour, A., Zeng, Z., Jiang, X., Van Dijk, A. I. J. M., and Miralles, D. G.: High-Resolution (1 Km) Köppen-Geiger Maps for 1901–2099 Based on Constrained CMIP6 Projections, Scientific Data, 10, 724, https://doi.org/10.1038/s41597-023-02549-6, 2023.

Berg, A. and Sheffield, J.: Evapotranspiration Partitioning in CMIP5 Models: Uncertainties and Future Projections, Journal of Climate, 32, 2653–2671, https://doi.org/10.1175/JCLI-D-18-0583.1, 2019.

Bergström, S.: The HBV Model, in: Computer Models of Watershed Hydrology, edited by Singh, V. P., pp. 443–476, Water Resources Publications, Highlands Ranch, Colorado, 1995.

Best, M. J., Abramowitz, G., Johnson, H. R., Pitman, A. J., Balsamo, G., Boone, A., Cuntz, M., Decharme, B., Dirmeyer, P. A., Dong, J., Ek, M., Guo, Z., Haverd, V., van den Hurk, B. J. J., Nearing, G. S., Pak, B., Peters-Lidard, C., Santanello Jr., J. A., Stevens, L., and Vuichard, N.: The Plumbing of Land Surface Models: Benchmarking Model Performance, Journal of Hydrometeorology, 16, 1425–1442, https://doi.org/10.1175/JHM-D-14-0158.1, 2015.

Beven, K. J. and Kirkby, M. J.: A Physically Based, Variable Contributing Area Model of Basin Hydrology / Un Modèle à Base Physique de Zone d'appel Variable de l'hydrologie Du Bassin Versant, Hydrological Sciences Bulletin, 24, 43–69, https://doi.org/10.1080/02626667909491834, 1979.

Bonan, G. B.: Forests and Climate Change: Forcings, Feedbacks, and the Climate Benefits of Forests, Science, 320, 1444–1449, https://doi.org/10.1126/science.1155121, 2008.

https://doi.org/10.5194/egusphere-2026-4223
Preprint. Discussion started: 28 July 2026

Boone, A., Samuelsson, P., Gollvik, S., Napoly, A., Jarlan, L., Brun, E., and Decharme, B.: The Interactions between Soil–Biosphere–Atmosphere Land Surface Model with a Multi-Energy Balance (ISBA-MEB) Option in SURFEXv8 – Part 1: Model Description, Geoscientific Model Development, 10, 843–872, https://doi.org/10.5194/gmd-10-843-2017, 2017.

Bowen, G. J., Cai, Z., Fiorella, R. P., and Putman, A. L.: Isotopes in the Water Cycle: Regional- to Global-Scale Patterns and Applications, Annual Review of Earth and Planetary Sciences, 47, 453–479, https://doi.org/10.1146/annurev-earth-053018-060220, 2019.

Calvet, J.-C., Rivalland, V., Picon-Cochard, C., and Guehl, J.-M.: Modelling Forest Transpiration and CO2 Fluxes—Response to Soil Moisture Stress, Agricultural and Forest Meteorology, 124, 143–156, https://doi.org/10.1016/j.agrformet.2004.01.007, 2004.

Campoy, A.: Influence de l'hydrologie souterraine sur la modélisation du climat à l'échelle régionale et globale, Ph.D. thesis, Dissertation (in French) Université Pierre et Marie Curie - Paris VI, France, 2013.

Chang, L.-L., Dwivedi, R., Knowles, J. F., Fang, Y.-H., Niu, G.-Y., Pelletier, J. D., Rasmussen, C., Durcik, M., Barron-Gafford, G. A., and Meixner, T.: Why Do Large-Scale Land Surface Models Produce a Low Ratio of Transpiration to Evapotranspiration?, Journal of Geophysical Research: Atmospheres, 123, 9109–9130, https://doi.org/10.1029/2018JD029159, 2018.

Chen, F. and Dudhia, J.: Coupling an Advanced Land Surface-Hydrology Model with the Penn State-NCAR MM5 Modeling System. Part I: Model Implementation and Sensitivity, Monthly Weather Review, 129, 569–585, https://doi.org/10.1175/1520-0493(2001)129<0569:CAALSH>2.0.CO;2, 2001.

Chen, T. H., Henderson-Sellers, A., Milly, P. C. D., Pitman, A. J., Beljaars, A. C. M., Polcher, J., Abramopoulos, F., Boone, A., Chang, S., Chen, F., Dai, Y., Desborough, C. E., Dickinson, R. E., Dümenil, L., Ek, M., Garratt, J. R., Gedney, N., Gusev, Y. M., Kim, J., Koster, R., Kowalczyk, E. A., Laval, K., Lean, J., Lettenmaier, D., Liang, X., Mahfouf, J.-F., Mengelkamp, H.-T., Mitchell, K., Nasonova, O. N., Noilhan, J., Robock, A., Rosenzweig, C., Schaake, J., Schlosser, C. A., Schulz, J.-P., Shao, Y., Shmakin, A. B., Verseghy, D. L., Wetzel, P., Wood, E. F., Xue, Y., Yang, Z.-L., and Zeng, Q.: Cabauw Experimental Results from the Project for Intercomparison of Land-Surface Parameterization Schemes, Journal of Climate, 10, 1194–1215, https://doi.org/10.1175/1520-0442(1997)010<1194:CERFTP>2.0.CO;2, 1997.

Clapp, R. B. and Hornberger, G. M.: Empirical Equations for Some Soil Hydraulic-Properties, Water Resources Research, 14, 601–604, https://doi.org/10.1029/WR014i004p00601, 1978.

Cuntz, M. and Haverd, V.: Physically Accurate Soil Freeze-Thaw Processes in a Global Land Surface Scheme, Journal of Advances in Modeling Earth Systems, 10, 54–77, https://doi.org/10.1002/2017MS001100, 2018.

Cuntz, M., Mai, J., Samaniego, L., Clark, M., Wulfmeyer, V., Branch, O., Attinger, S., and Thober, S.: The Impact of Standard and Hard-Coded Parameters on the Hydrologic Fluxes in the Noah-MP Land Surface Model, Journal of Geophysical Research: Atmospheres, 121, 10 676–10 700, https://doi.org/10.1002/2016JD025097, 2016.

Cuntz, M., Thober, S., Verhoef, A., Zeng, Y., Boone, A., Ducharne, A., Koirala, S., Lawrence, D. M., de Vrese, P., Montzka, C., Seneviratne, S. I., Vereecken, H., Or, D., Tafasca, S., Mizukami, N., Ellis, R., McGuire, P. C., and Gudmundsson, L.: Soil Parameter Model Intercomparison Project (SP-MIP): Assessing the Influence of Soil Parameters on the Variability of Land Surface Models - Mean Output Files and Plotting Scripts, Zenodo, https://doi.org/10.5281/zenodo.21473084, 2026.

De Kauwe, M. G., Medlyn, B. E., Ukkola, A. M., Mu, M., Sabot, M. E. B., Pitman, A. J., Meir, P., Cernusak, L. A., Rifai, S. W., Choat, B., Tissue, D. T., Blackman, C. J., Li, X., Roderick, M., and Briggs, P. R.: Identifying Areas at Risk of Drought-Induced Tree Mortality across South-Eastern Australia, Global Change Biology, 26, 5716–5733, https://doi.org/10.1111/gcb.15215, 2020.

Decharme, B. and Douville, H.: Introduction of a Sub-Grid Hydrology in the ISBA Land Surface Model, Climate Dynamics, 26, 65–78, https://doi.org/10.1007/s00382-005-0059-7, 2006.

https://doi.org/10.5194/egusphere-2026-4223
Preprint. Discussion started: 28 July 2026

Decharme, B., Delire, C., Minvielle, M., Colin, J., Vergnes, J.-P., Alias, A., Saint-Martin, D., Séférian, R., Sénési, S., and Voldoire, A.: Recent Changes in the ISBA-CTRIP Land Surface System for Use in the CNRM-CM6 Climate Model and in Global Off-Line Hydrological Applications, Journal of Advances in Modeling Earth Systems, 11, 1207–1252, https://doi.org/10.1029/2018MS001545, 2019.

Dirmeyer, P. A., Gao, X., Zhao, M., Guo, Z., Oki, T., and Hanasaki, N.: GSWP-2: Multimodel Analysis and Implications for Our Perception of the Land Surface, Bulletin of the American Meteorological Society, 87, 1381–1398, https://doi.org/10.1175/BAMS-87-10-1381, 2006.

d'Orgeval, T., Polcher, J., and de Rosnay, P.: Sensitivity of the West African Hydrological Cycle in ORCHIDEE to Infiltration Processes, Hydrology and Earth System Sciences, 12, 1387–1401, https://doi.org/10.5194/hess-12-1387-2008, 2008.

Dümenil, L. and Todini, E.: A Rainfall–Runoff Scheme for Use in the Hamburg Climate Model, in: Advances in Theoretical Hydrology, edited by O'Kane, J. P., European Geophysical Society Series on Hydrological Sciences, pp. 129–157, Elsevier, Amsterdam, 1992.

Egea, G., Verhoef, A., and Vidale, P. L.: Towards an Improved and More Flexible Representation of Water Stress in Coupled Photosynthesis-Stomatal Conductance Models, Agricultural and Forest Meteorology, 151, 1370–1384, https://doi.org/10.1016/j.agrformet.2011.05.019, 2011.

Eyring, V., Bony, S., Meehl, G. A., Senior, C. A., Stevens, B., Stouffer, R. J., and Taylor, K. E.: Overview of the Coupled Model Intercomparison Project Phase 6 (CMIP6) Experimental Design and Organization, Geoscientific Model Development, 9, 1937–1958, https://doi.org/10.5194/gmd-9-1937-2016, 2016.

Farquhar, G. D., Von Caemmerer, S., and Berry, J. A.: A Biochemical Model of Photosynthetic CO2 Assimilation in Leaves of C3 Species, Planta, 149, 78–90, https://doi.org/10.1007/BF00386231, 1980.

Feigl, M., Thober, S., Schweppe, R., Herrnegger, M., Samaniego, L., and Schulz, K.: Automatic Regionalization of Model Parameters for Hydrological Models, Water Resources Research, 58, e2022WR031 966, https://doi.org/10.1029/2022WR031966, 2022.

Freschet, G. T., Violle, C., Roumet, C., and Garnier, É.: Interactions between Soil and Vegetation: Structure of Plant Communities and Soil Functioning, in: Soils as a Key Component of the Critical Zone 6, edited by Lemanceau, P. and Blouin, M., pp. 83–104, Wiley, 1 edn., ISBN 978-1-119-43827-4, https://doi.org/10.1002/9781119438274.ch5, 2018.

Friedlingstein, P., Cox, P. M., Betts, R. A., Bopp, L., von Bloh, W., Brovkin, V., Cadule, P., Doney, S. C., Eby, M., Fung, I. Y., Bala, G., John, J., Jones, C., Joos, F., Kato, T., Kawamiya, M., Knorr, W., Lindsay, K., Matthews, H. D., Raddatz, T. J., Rayner, P. J., Reick, C. H., Roeckner, E., Schnitzler, K. G., Schnur, R., Strassmann, K., Weaver, A. J., Yoshikawa, C., and Zeng, N.: Climate-Carbon Cycle Feedback Analysis: Results from the (CMIP)-M-4 Model Intercomparison, Journal of Climate, 19, 3337–3353, 2006.

Fu, Z., Ciais, P., Feldman, A. F., Gentine, P., Makowski, D., Prentice, I. C., Stoy, P. C., Bastos, A., and Wigneron, J.-P.: Critical Soil Moisture Thresholds of Plant Water Stress in Terrestrial Ecosystems, Science Advances, 8, https://doi.org/10.1126/sciadv.abq7827, 2022a.

Fu, Z., Ciais, P., Makowski, D., Bastos, A., Stoy, P. C., Ibrom, A., Knohl, A., Migliavacca, M., Cuntz, M., Šigut, L., Peichl, M., Loustau, D., El-Madany, T. S., Buchmann, N., Gharun, M., Janssens, I., Markwitz, C., Grünwald, T., Rebmann, C., Mölder, M., Varlagin, A., Mammarella, I., Kolari, P., Bernhofer, C., Heliasz, M., Vincke, C., Pitacco, A., Cremonese, E., Foltýnová, L., and Wigneron, J.-P.: Uncovering the Critical Soil Moisture Thresholds of Plant Water Stress for European Ecosystems, Global Change Biology, 28, 2111–2123, https://doi.org/10.1111/gcb.16050, 2022b.

Garcia Gonzalez, R., Verhoef, A., Luigi Vidale, P., and Braud, I.: Incorporation of Water Vapor Transfer in the JULES Land Surface Model: Implications for Key Soil Variables and Land Surface Fluxes, Water Resources Research, 48, W05 538, https://doi.org/10.1029/2011WR011811, 2012.

Giorgetta, M. A., Roeckner, E., Mauritsen, T., Bader, J., Crueger, T., Esch, M., Rast, S., Kornblueh, L., Schmidt, H., Kinne, S., Hohenegger, C., Möbis, B., Krismer, T., Wieners, K.-H., and Stevens, B.: The Atmospheric General Circulation Model ECHAM6 - Model Description, Reports on Earth System Science, Max Planck Institute for Meteorology, Hamburg, Germany, 135, 172, 2013.

Göhler, M., Mai, J., and Cuntz, M.: Use of Eigendecomposition in a Parameter Sensitivity Analysis of the Community Land Model, Journal of Geophysical Research, 118, 904–921, https://doi.org/10.1002/jgrg.20072, 2013.

Gudmundsson, L. and Cuntz, M.: Soil Parameter Model Intercomparison Project (SP-MIP): Assessing the Influence of Soil Parameters on the Variability of Land Surface Models - Soil Input Files and Simulation Protocol, Zenodo, https://doi.org/10.5281/zenodo.21469535, 2017.

Hagemann, S. and Stacke, T.: Impact of the Soil Hydrology Scheme on Simulated Soil Moisture Memory, Climate Dynamics, 44, 1731–1750, https://doi.org/10.1007/s00382-014-2221-6, 2015.

Hare, D. K., Helton, A. M., Johnson, Z. C., Lane, J. W., and Briggs, M. A.: Continental-Scale Analysis of Shallow and Deep Groundwater Contributions to Streams, Nature Communications, 12, 1450, https://doi.org/10.1038/s41467-021-21651-0, 2021.

Haughton, N., Abramowitz, G., Pitman, A. J., Or, D., Best, M. J., Johnson, H. R., Balsamo, G., Boone, A., Cuntz, M., Decharme, B., Dirmeyer, P. A., Dong, J., Ek, M., Guo, Z., Haverd, V., van den Hurk, B. J. J., Nearing, G. S., Pak, B., Santanello Jr., J. A., Stevens, L. E., and Vuichard, N.: The Plumbing of Land Surface Models: Is Poor Performance a Result of Methodology or Data Quality?, Journal of Hydrometeorology, 17, 1705–1723, https://doi.org/10.1175/JHM-D-15-0171.1, 2016.

Haverd, V. and Cuntz, M.: Soil-Litter-Iso: A One-Dimensional Model for Coupled Transport of Heat, Water and Stable Isotopes in Soil with a Litter Layer and Root Extraction, Journal of Hydrology, 388, 438–455, https://doi.org/10.1016/j.jhydrol.2010.05.029, 2010.

Heber Green, W. and Ampt, G. A.: Studies on Soil Physics, The Journal of Agricultural Science, 4, 1–24, https://doi.org/10.1017/S0021859600001441, 1911.

Henderson-Sellers, A., McGuffie, K., and Pitman, A. J.: The Project for Intercomparison of Land-surface Parametrization Schemes (PILPS): 1992 to 1995:, Climate Dynamics, 12, 849–859, https://doi.org/10.1007/s003820050147, 1996.

Hengl, T., de Jesus, J. M., MacMillan, R. A., Batjes, N. H., Heuvelink, G. B. M., Ribeiro, E., Samuel-Rosa, A., Kempen, B., Leenaars, J. G. B., Walsh, M. G., and Gonzalez, M. R.: SoilGrids1km — Global Soil Information Based on Automated Mapping, PLoS ONE, 9, e105 992, https://doi.org/10.1371/journal.pone.0105992, 2014.

Huntzinger, D. N., Schwalm, C., Michalak, A. M., Schaefer, K., King, A. W., Wei, Y., Jacobson, A., Liu, S., Cook, R. B., Post, W. M., Berthier, G., Hayes, D., Huang, M., Ito, A., Lei, H., Lu, C., Mao, J., Peng, C. H., Peng, S., Poulter, B., Riccuito, D., Shi, X., Tian, H., Wang, W., Zeng, N., Zhao, F., and Zhu, Q.: The North American Carbon Program Multi-Scale Synthesis and Terrestrial Model Intercomparison Project – Part 1: Overview and Experimental Design, Geoscientific Model Development, 6, 2121–2133, https://doi.org/10.5194/gmd-6-2121-2013, 2013.

IPCC: Climate Change 2021: The Physical Science Basis. Contribution of Working Group I to the Sixth Assessment Report of the Intergovernmental Panel on Climate Change, Cambridge University Press, Cambridge, United Kingdom and New York, NY, USA, https://doi.org/10.1017/9781009157896, 2021.

Jacobs, C.: Direct Impact of Atmospheric CO2 Enrichment on Regional Transpiration, Ph.D. thesis, Landbouwuniversiteit Wageningen, Wageningen, ISBN 9789054852506, 1994.

Jasechko, S., Kirchner, J. W., Welker, J. M., and McDonnell, J. J.: Substantial Proportion of Global Streamflow Less than Three Months Old, Nature Geoscience, 9, 126–129, https://doi.org/10.1038/ngeo2636, 2016.

Joetzjer, E., Delire, C., Douville, H., Ciais, P., Decharme, B., Carrer, D., Verbeeck, H., De Weirdt, M., and Bonal, D.: Improving the ISBA$_{CC}$ Land Surface Model Simulation of Water and Carbon Fluxes and Stocks over the Amazon Forest, Geoscientific Model Development, 8, 1709–1727, https://doi.org/10.5194/gmd-8-1709-2015, 2015.

Kattge, J., Díaz, S., Lavorel, S., Prentice, I. C., Leadley, P., Bönisch, G., Garnier, E., Westoby, M., Reich, P. B., Wright, I. J., Cornelissen, J. H. C., Violle, C., Harrison, S. P., Van Bodegom, P. M., Reichstein, M., Enquist, B. J., Soudzilovskaia, N. A., Ackerly, D. D., Anand, M., Atkin, O. K., Bahn, M., Baker, T. R., Baldocchi, D., Bekker, R., Blanco, C. C., Blonder, B., Bond, W. J., Bradstock, R., Bunker, D. E., Casanoves, F., Cavender-Bares, J., Chambers, J. Q., Chapin Iii, F. S., Chave, J., Coomes, D., Cornwell, W. K., Craine, J. M., Dobrin, B. H., Duarte, L., Durka, W., Elser, J., Esser, G., Estiarte, M., Fagan, W. F., Fang, J., Fernández-Méndez, F., Fidelis, A., Finegan, B., Flores, O., Ford, H., Frank, D., Freschet, G. T., Fyllas, N. M., Gallagher, R. V., Green, W. A., Gutierrez, A. G., Hickler, T., Higgins, S. I., Hodgson, J. G., Jalili, A., Jansen, S., Joly, C. A., Kerkhoff, A. J., Kirkup, D., Kitajima, K., Kleyer, M., Klotz, S., Knops, J. M. H., Kramer, K., Kühn, I., Kurokawa, H., Laughlin, D., Lee, T. D., Leishman, M., Lens, F., Lenz, T., Lewis, S. L., Lloyd, J., Llusià, J., Louault, F., Ma, S., Mahecha, M. D., Manning, P., Massad, T., Medlyn, B. E., Messier, J., Moles, A. T., Müller, S. C., Nadrowski, K., Naeem, S., Niinemets, Ü., Nöllert, S., Nüske, A., Ogaya, R., Oleksyn, J., Onipchenko, V. G., Onoda, Y., Ordoñez, J., Overbeck, G., Ozinga, W. A., Patiño, S., Paula, S., Pausas, J. G., Peñuelas, J., Phillips, O. L., Pillar, V., Poorter, H., Poorter, L., Poschlod, P., Prinzing, A., Proulx, R., Rammig, A., Reinsch, S., Reu, B., Sack, L., Salgado-Negret, B., Sardans, J., Shiodera, S., Shipley, B., Siefert, A., Sosinski, E., Soussana, J.-F., Swaine, E., Swenson, N., Thompson, K., Thornton, P., Waldram, M., Weiher, E., White, M., White, S., Wright, S. J., Yguel, B., Zaehle, S., Zanne, A. E., and Wirth, C.: TRY - a Global Database of Plant Traits, Global Change Biology, 17, 2905–2935, https://doi.org/10.1111/j.1365-2486.2011.02451.x, 2011.

Kattge, J., Bönisch, G., Diaz, S., Lavorel, S., Prentice, I. C., Leadley, P., Tautenhahn, S., Werner, G. D. A., Aakala, T., Abedi, M., Acosta, A. T. R., Adamidis, G. C., Adamson, K., Aiba, M., Albert, C. H., Alcántara, J. M., Alcázar C, C., Aleixo, I., Ali, H., Amiaud, B., Ammer, C., Amoroso, M. M., Anand, M., Anderson, C., Anten, N., Antos, J., Apgaua, D. M. G., Ashman, T.-L., Asmara, D. H., Asner, G. P., Aspinwall, M., Atkin, O., Aubin, I., Baastrup-Spohr, L., Bahalkeh, K., Bahn, M., Baker, T., Baker, W. J., Bakker, J. P., Baldocchi, D., Baltzer, J., Banerjee, A., Baranger, A., Barlow, J., Barneche, D. R., Baruch, Z., Bastianelli, D., Battles, J., Bauerle, W., Bauters, M., Bazzato, E., Beckmann, M., Beeckman, H., Beierkuhnlein, C., Bekker, R., Belfry, G., Belluau, M., Beloiu, M., Benavides, R., Benomar, L., Berdugo-Lattke, M. L., Berenguer, E., Bergamin, R., Bergmann, J., Bergmann Carlucci, M., Berner, L., Bernhardt-Römermann, M., Bigler, C., Bjorkman, A. D., Blackman, C., Blanco, C., Blonder, B., Blumenthal, D., Bocanegra-González, K. T., Boeckx, P., Bohlman, S., Böhning-Gaese, K., Boisvert-Marsh, L., Bond, W., Bond-Lamberty, B., Boom, A., Boonman, C. C. F., Bordin, K., Boughton, E. H., Boukili, V., Bowman, D. M. J. S., Bravo, S., Brendel, M. R., Broadley, M. R., Brown, K. A., Bruelheide, H., Brumnich, F., Bruun, H. H., Bruy, D., Buchanan, S. W., Bucher, S. F., Buchmann, N., Buitenwerf, R., Bunker, D. E., Bürger, J., Burrascano, S., Burslem, D. F. R. P., Butterfield, B. J., Byun, C., Marques, M., Scalon, M. C., Caccianiga, M., Cadotte, M., Cailleret, M., Camac, J., Camarero, J. J., Campany, C., Campetella, G., Campos, J. A., Cano-Arboleda, L., Canullo, R., Carbognani, M., Carvalho, F., Casanoves, F., Castagneyrol, B., Catford, J. A., Cavender-Bares, J., Cerabolini, B. E. L., Cervellini, M., Chacón-Madrigal, E., Chapin, K., Chapin, F. S., Chelli, S., Chen, S.-C., Chen, A., Cherubini, P., Chianucci, F., Choat, B., Chung, K.-S., Chytrý, M., Ciccarelli, D., Coll, L., Collins, C. G., Conti, L., Coomes, D., Cornelissen, J. H. C., Cornwell, W. K., Corona, P., Coyea, M., Craine, J., Craven, D., Cromsigt, J. P. G. M., Csecserits, A., Čufar, K., Cuntz, M., Silva, A. C., Dahlin, K. M., Dainese, M., Dalke, I., Dalle Fratte, M., Dang-Le, A. T., Danihelka, J., Dannoura, M., Dawson, S., Beer, A. J., De Frutos, A., De Long, J. R., Dechant, B., Delagrange, S., Delpierre, N., Derroire, G., Dias, A. S., Diaz-Toribio, M. H., Dimitrakopoulos, P. G., Dobrowolski, M., Doktor, D., Dřevojan, P., Dong, N., Dransfield, J., Dressler, S., Duarte, L., Ducouret, E., Dullinger, S., Durka, W., Duursma, R., Dymova, O., E-Vojtkó, A., Eckstein, R. L., Ejtehadi, H., Elser, J., Emilio, T., Engemann, K.,

https://doi.org/10.5194/egusphere-2026-4223
Preprint. Discussion started: 28 July 2026

Erfanian, M. B., Erfmeier, A., Esquivel-Muelbert, A., Esser, G., Estiarte, M., Domingues, T. F., Fagan, W. F., Fagúndez, J., Falster, D. S., Fan, Y., Fang, J., Farris, E., Fazlioglu, F., Feng, Y., Fernandez-Mendez, F., Ferrara, C., Ferreira, J., Fidelis, A., Finegan, B., Firn, J., Flowers, T. J., Flynn, D. F. B., Fontana, V., Forey, E., Forgiarini, C., Francois, L., Frangipani, M., Frank, D., Frenette-Dussault, C., Freschet, G. T., Fry, E. L., Fyllas, N. M., Mazzochini, G. G., Gachet, S., Gallagher, R., Ganade, G., Ganga, F., García-Palacios, P., Gargaglione, V., Garnier, E., Garrido, J. L., Gasper, A. L., Gea-Izquierdo, G., Gibson, D., Gillison, A. N., Giroldo, A., Glasenhardt, M.-C., Gleason, S., Gliesch, M., Goldberg, E., Göldel, B., Gonzalez-Akre, E., Gonzalez-Andujar, J. L., González-Melo, A., González-Robles, A., Graae, B. J., Granda, E., Graves, S., Green, W. A., Gregor, T., Gross, N., Guerin, G. R., Günther, A., Gutiérrez, A. G., Haddock, L., Haines, A., Hall, J., Hambuckers, A., Han, W., Harrison, S. P., Hattingh, W., Hawes, J. E., He, T., He, P., Heberling, J. M., Helm, A., Hempel, S., Hentschel, J., Hérault, B., Hereş, A.-M., Herz, K., Heuertz, M., Hickler, T., Hietz, P., Higuchi, P., Hipp, A. L., Hirons, A., Hock, M., Hogan, J. A., Holl, K., Honnay, O., Hornstein, D., Hou, E., Hough-Snee, N., Hovstad, K. A., Ichie, T., Igić, B., Illa, E., Isaac, M., Ishihara, M., Ivanov, L., Ivanova, L., Iversen, C. M., Izquierdo, J., Jackson, R. B., Jackson, B., Jactel, H., Jagodzinski, A. M., Jandt, U., Jansen, S., Jenkins, T., Jentsch, A., Jespersen, J. R. P., Jiang, G.-F., Johansen, J. L., Johnson, D., Jokela, E. J., Joly, C. A., Jordan, G. J., Joseph, G. S., Junaedi, D., Junker, R. R., Justes, E., Kabzems, R., Kane, J., Kaplan, Z., Kattenborn, T., Kavelenova, L., Kearsley, E., Kempel, A., Kenzo, T., Kerkhoff, A., Khalil, M. I., Kinlock, N. L., Kissling, W. D., Kitajima, K., Kitzberger, T., Kjøller, R., Klein, T., Kleyer, M., Klimešová, J., Klipel, J., Kloeppel, B., Klotz, S., Knops, J. M. H., Kohyama, T., Koike, F., Kollmann, J., Komac, B., Komatsu, K., König, C., Kraft, N. J. B., Kramer, K., Kreft, H., Kühn, I., Kumarathunge, D., Kuppler, J., Kurokawa, H., Kurosawa, Y., Kuyah, S., Laclau, J.-P., Lafleur, B., Lallai, E., Lamb, E., Lamprecht, A., Larkin, D. J., Laughlin, D., Le Bagousse-Pinguet, Y., Maire, G., Roux, P. C., Roux, E., Lee, T., Lens, F., Lewis, S. L., Lhotsky, B., Li, Y., Li, X., Lichstein, J. W., Liebergesell, M., Lim, J. Y., Lin, Y.-S., Linares, J. C., Liu, C., Liu, D., Liu, U., Livingstone, S., Llusià, J., Lohbeck, M., López-García, Á., Lopez-Gonzalez, G., Lososová, Z., Louault, F., Lukács, B. A., Lukeš, P., Luo, Y., Lussu, M., Ma, S., Maciel Rabelo Pereira, C., Mack, M., Maire, V., Mäkelä, A., Mäkinen, H., Malhado, A. C. M., Mallik, A., Manning, P., Manzoni, S., Marchetti, Z., Marchino, L., Marcilio-Silva, V., Marcon, E., Marignani, M., Markesteijn, L., Martin, A., Martínez-Garza, C., Martínez-Vilalta, J., Mašková, T., Mason, K., Mason, N., Massad, T. J., Masse, J., Mayrose, I., McCarthy, J., McCormack, M. L., McCulloh, K., McFadden, I. R., McGill, B. J., McPartland, M. Y., Medeiros, J. S., Medlyn, B., Meerts, P., Mehrabi, Z., Meir, P., Melo, F. P. L., Mencuccini, M., Meredieu, C., Messier, J., Mészáros, I., Metsaranta, J., Michaletz, S. T., Michelaki, C., Migalina, S., Milla, R., Miller, J. E. D., Minden, V., Ming, R., Mokany, K., Moles, A. T., Molnár V, A., Molofsky, J., Molz, M., Montgomery, R. A., Monty, A., Moravcová, L., Moreno-Martínez, A., Moretti, M., Mori, A. S., Mori, S., Morris, D., Morrison, J., Mucina, L., Mueller, S., Muir, C. D., Müller, S. C., Munoz, F., Myers-Smith, I. H., Myster, R. W., Nagano, M., Naidu, S., Narayanan, A., Natesan, B., Negoita, L., Nelson, A. S., Neuschulz, E. L., Ni, J., Niedrist, G., Nieto, J., Niinemets, Ü., Nolan, R., Nottebrock, H., Nouvellon, Y., Novakovskiy, A., The Nutrient Network, Nystuen, K. O., O'Grady, A., O'Hara, K., O'Reilly-Nugent, A., Oakley, S., Oberhuber, W., Ohtsuka, T., Oliveira, R., Öllerer, K., Olson, M. E., Onipchenko, V., Onoda, Y., Onstein, R. E., Ordonez, J. C., Osada, N., Ostonen, I., Ottaviani, G., Otto, S., Overbeck, G. E., Ozinga, W. A., Pahl, A. T., Paine, C. E. T., Pakeman, R. J., Papageorgiou, A. C., Parfionova, E., Pärtel, M., Patacca, M., Paula, S., Paule, J., Pauli, H., Pausas, J. G., Peco, B., Peñuelas, J., Perea, A., Peri, P. L., Petisco-Souza, A. C., Petraglia, A., Petritan, A. M., Phillips, O. L., Pierce, S., Pillar, V. D., Pisek, J., Pomogaybin, A., Poorter, H., Portsmuth, A., Poschlod, P., Potvin, C., Pounds, D., Powell, A. S., Power, S. A., Prinzing, A., Puglielli, G., Pyšek, P., Raevel, V., Rammig, A., Ransijn, J., Ray, C. A., Reich, P. B., Reichstein, M., Reid, D. E. B., Réjou-Méchain, M., Dios, V. R., Ribeiro, S., Richardson, S., Riibak, K., Rillig, M. C., Riviera, F., Robert, E. M. R., Roberts, S., Robroek, B., Roddy, A., Rodrigues, A. V., Rogers, A., Rollinson, E., Rolo, V., Römermann, C., Ronzhina, D., Roscher, C., Rosell, J. A., Rosenfield, M. F., Rossi, C., Roy, D. B., Royer-Tardif, S., Rüger, N., Ruiz-Peinado, R., Rumpf, S. B., Rusch, G. M., Ryo, M., Sack, L., Saldaña, A., Salgado-Negret, B., Salguero-Gomez, R., Santa-Regina, I., Santacruz-García, A. C., Santos, J., Sardans, J., Schamp, B.,

https://doi.org/10.5194/egusphere-2026-4223
Preprint. Discussion started: 28 July 2026

Scherer-Lorenzen, M., Schleuning, M., Schmid, B., Schmidt, M., Schmitt, S., Schneider, J. V., Schowanek, S. D., Schrader, J., Schrodt, F., Schuldt, B., Schurr, F., Selaya Garvizu, G., Semchenko, M., Seymour, C., Sfair, J. C., Sharpe, J. M., Sheppard, C. S., Sheremetiev, S., Shiodera, S., Shipley, B., Shovon, T. A., Siebenkäs, A., Sierra, C., Silva, V., Silva, M., Sitzia, T., Sjöman, H., Slot, M., Smith, N. G., Sodhi, D., Soltis, P., Soltis, D., Somers, B., Sonnier, G., Sørensen, M. V., Sosinski Jr, E. E., Soudzilovskaia, N. A., Souza, A. F., Spasojevic, M., Sperandii, M. G., Stan, A. B., Stegen, J., Steinbauer, K., Stephan, J. G., Sterck, F., Stojanović, D. B., Strydom, T., Suarez, M. L., Svenning, J.-C., Svitková, I., Svitok, M., Svoboda, M., Swaine, E., Swenson, N., Tabarelli, M., Takagi, K., Tappeiner, U., Tarifa, R., Tauugourdeau, S., Tavsanoglu, C., Beest, M., Tedersoo, L., Thiffault, N., Thom, D., Thomas, E., Thompson, K., Thornton, P. E., Thuiller, W., Tichý, L., Tissue, D., Tjoelker, M. G., Tng, D. Y. P., Tobias, J., Török, P., Tarin, T., Torres-Ruiz, J. M., Tóthmérész, B., Treurnicht, M., Trivellone, V., Trolliet, F., Trotsiuk, V., Tsakalos, J. L., Tsiripidis, I., Tysklind, N., Umehara, T., Usoltsev, V., Vadeboncoeur, M., Vaezi, J., Valladares, F., Vamosi, J., Bodegom, P. M., Breugel, M., Van Cleemput, E., Weg, M., Merwe, S., Plas, F., Sande, M. T., Kleunen, M., Van Meerbeek, K., Vanderwel, M., Vanselow, K. A., V\aarhammar, A., Varone, L., Vasquez Valderrama, M. Y., Vassilev, K., Vellend, M., Veneklaas, E. J., Verbeeck, H., Verheyen, K., Vibrans, A., Vieira, I., Villacís, J., Violle, C., Vivek, P., Wagner, K., Waldram, M., Waldron, A., Walker, A. P., Waller, M., Walther, G., Wang, H., Wang, F., Wang, W., Watkins, H., Watkins, J., Weber, U., Weedon, J. T., Wei, L., Weigelt, P., Weiher, E., Wells, A. W., Wellstein, C., Wenk, E., Westoby, M., Westwood, A., White, P. J., Whitten, M., Williams, M., Winkler, D. E., Winter, K., Womack, C., Wright, I. J., Wright, S. J., Wright, J., Pinho, B. X., Ximenes, F., Yamada, T., Yamaji, K., Yanai, R., Yankov, N., Yguel, B., Zanini, K. J., Zanne, A. E., Zelený, D., Zhao, Y.-P., Zheng, J., Zheng, J., Ziemińska, K., Zirbel, C. R., Zizka, G., Zo-Bi, I. C., Zotz, G., and Wirth, C.: TRY Plant Trait Database – Enhanced Coverage and Open Access, Global Change Biology, 26, 119–188, https://doi.org/10.1111/gcb.14904, 2020.

Kennedy, D., Swenson, S., Oleson, K. W., Lawrence, D. M., Fisher, R., Lola Da Costa, A. C., and Gentine, P.: Implementing Plant Hydraulics in the Community Land Model, Version 5, Journal of Advances in Modeling Earth Systems, 11, 485–513, https://doi.org/10.1029/2018MS001500, 2019.

Koirala, S., Oki, T., and Kanae, S.: Fully Dynamic Groundwater Representation in the MATSIRO Land Surface Model, Annual Journal of Hydraulic Engineering, Japanese Society of Civil Engineering, 54, 37–42, 2010.

Koirala, S., Yeh, P. J.-F., Hirabayashi, Y., Kanae, S., and Oki, T.: Global-scale Land Surface Hydrologic Modeling with the Representation of Water Table Dynamics, Journal of Geophysical Research: Atmospheres, 119, 75–89, https://doi.org/10.1002/2013JD020398, 2014.

Lawrence, D. M., Fisher, R. A., Koven, C. D., Oleson, K. W., Swenson, S. C., Vertenstein, M., Andre, B., Bonan, G. B., Ghimire, B., van Kampenhout, L., Kennedy, D., Kluzek, E., Knox, R., Lawrence, P., Li, F., Li, H., Lombardozzi, D., Lu, Y., Perket, J., Riley, W., Sacks, W., Shi, M., Wieder, W., Xu, C., Ali, A., Badger, A., Bisht, G., Broxton, P., Brunke, M., Buzan, J., Clark, M., Craig, T., Dahlin, K., Drewniak, B., Emmons, L., Fisher, J., Flanner, M., Gentine, P., Lenaerts, J., Levis, S., Leung, L. R., Lipscomb, W., Pelletier, J., Ricciuto, D. M., Sanderson, B., Shuman, J., Slater, A., Subin, Z., Tang, J., Tawfik, A., Thomas, Q., Tilmes, S., Vitt, F., and Zeng, X.: Technical Description of Version 5.0 of the Community Land Model (CLM), Tech. rep., National Center for Atmospheric Research (NCAR), Boulder, CO, 2018.

Lawrence, D. M., Fisher, R. A., Koven, C. D., Oleson, K. W., Swenson, S. C., Bonan, G., Collier, N., Ghimire, B., van Kampenhout, L., Kennedy, D., Kluzek, E., Lawrence, P. J., Li, F., Li, H., Lombardozzi, D., Riley, W. J., Sacks, W. J., Shi, M., Vertenstein, M., Wieder, W. R., Xu, C., Ali, A. A., Badger, A. M., Bisht, G., van den Broeke, M., Brunke, M. A., Burns, S. P., Buzan, J., Clark, M., Craig, A., Dahlin, K., Drewniak, B., Fisher, J. B., Flanner, M., Fox, A. M., Gentine, P., Hoffman, F., Keppel-Aleks, G., Knox, R., Kumar, S., Lenaerts, J., Leung, L. R., Lipscomb, W. H., Lu, Y., Pandey, A., Pelletier, J. D., Perket, J., Randerson, J. T., Ricciuto, D. M., Sanderson, B. M., Slater, A., Subin, Z. M., Tang, J., Thomas, R. Q., Val Martin, M., and Zeng, X.: The Community Land Model Version 5: Description

https://doi.org/10.5194/egusphere-2026-4223
Preprint. Discussion started: 28 July 2026

of New Features, Benchmarking, and Impact of Forcing Uncertainty, Journal of Advances in Modeling Earth Systems, 11, 4245–4287, https://doi.org/10.1029/2018MS001583, 2019.

Lehmann, P., Berli, M., Koonce, J. E., and Or, D.: Surface Evaporation in Arid Regions: Insights From Lysimeter Decadal Record and Global Application of a Surface Evaporation Capacitor (SEC) Model, Geophysical Research Letters, 46, 9648–9657, https://doi.org/10.1029/2019GL083932, 2019.

Li, K. Y., de Jong, R., and Boisvert, J. B.: An Exponential Root-Water-Uptake Model with Water Stress Compensation, Journal of Hydrology, 252, 189–204, 2001.

Lian, X., Piao, S., Huntingford, C., Li, Y., Zeng, Z., Wang, X., Ciais, P., McVicar, T. R., Peng, S., Ottlé, C., Yang, H., Yang, Y., Zhang, Y., and Wang, T.: Partitioning Global Land Evapotranspiration Using CMIP5 Models Constrained by Observations, Nature Climate Change, 8, 640–646, https://doi.org/10.1038/s41558-018-0207-9, 2018.

Liang, X., Lettenmaier, D. P., Wood, E. F., and Burges, S. J.: A Simple Hydrologically Based Model of Land Surface Water and Energy Fluxes for General Circulation Models, Journal of Geophysical Research: Atmospheres, 99, 14 415–14 428, https://doi.org/10.1029/94JD00483, 1994.

Liang, X., Wood, E. F., Lettenmaier, D. P., Lohmann, D., Boone, A., Chang, S., Chen, F., Dai, Y., Desborough, C., Dickinson, R. E., Duan, Q., Ek, M., Gusev, Y. M., Habets, F., Irannejad, P., Koster, R., Mitchell, K. E., Nasonova, O. N., Noilhan, J., Schaake, J., Schlosser, A., Shao, Y., Shmakin, A. B., Verseghy, D., Warrach, K., Wetzel, P., Xue, Y., Yang, Z.-L., and Zeng, Q.-c.: The Project for Intercomparison of Land-Surface Parameterization Schemes (PILPS) Phase 2(c) Red–Arkansas River Basin Experiment: 2. Spatial and Temporal Analysis of Energy Fluxes, Global and Planetary Change, 19, 137–159, https://doi.org/10.1016/S0921-8181(98)00045-9, 1998.

Lindström, G., Pers, C., Rosberg, J., Strömqvist, J., and Arheimer, B.: Development and Testing of the HYPE (Hydrological Predictions for the Environment) Water Quality Model for Different Spatial Scales, Hydrology Research, 41, 295–319, https://doi.org/10.2166/nh.2010.007, 2010.

Liu, J.-F., Arend, M., Yang, W.-J., Schaub, M., Ni, Y.-Y., Gessler, A., Jiang, Z.-P., Rigling, A., and Li, M.-H.: Effects of Drought on Leaf Carbon Source and Growth of European Beech Are Modulated by Soil Type, Scientific Reports, 7, 42 462, https://doi.org/10.1038/srep42462, 2017.

Liu, L., Gudmundsson, L., Hauser, M., Qin, D., Li, S., and Seneviratne, S. I.: Soil Moisture Dominates Dryness Stress on Ecosystem Production Globally, Nature Communications, 11, 4892, https://doi.org/10.1038/s41467-020-18631-1, 2020.

Lohmann, D., Lettenmaier, D. P., Liang, X., Wood, E. F., Boone, A., Chang, S., Chen, F., Dai, Y., Desborough, C., Dickinson, R. E., Duan, Q., Ek, M., Gusev, Y. M., Habets, F., Irannejad, P., Koster, R., Mitchell, K. E., Nasonova, O. N., Noilhan, J., Schaake, J., Schlosser, A., Shao, Y., Shmakin, A. B., Verseghy, D., Warrach, K., Wetzel, P., Xue, Y., Yang, Z.-L., and Zeng, Q.-c.: The Project for Intercomparison of Land-Surface Parameterization Schemes (PILPS) Phase 2(c) Red–Arkansas River Basin Experiment: 3. Spatial and Temporal Analysis of Water Fluxes, Global and Planetary Change, 19, 161–179, https://doi.org/10.1016/S0921-8181(98)00046-0, 1998.

MacBean, N., Scott, R. L., Biederman, J. A., Ottlé, C., Vuichard, N., Ducharne, A., Kolb, T., Dore, S., Litvak, M., and Moore, D. J. P.: Testing Water Fluxes and Storage from Two Hydrology Configurations within the ORCHIDEE Land Surface Model across US Semi-Arid Sites, Hydrology and Earth System Sciences, 24, 5203–5230, https://doi.org/10.5194/hess-24-5203-2020, 2020.

Martí, B., Groh, J., Canut, G., and Boone, A.: Implementation of a Dry Surface Layer Soil Resistance in Two Contrasting Semi-Arid Sites with SURFEX-ISBA V9.0, EGUsphere, 2025, 1–43, https://doi.org/10.5194/egusphere-2025-1783, 2025.

Medlyn, B. E., Duursma, R. A., Eamus, D., Ellsworth, D. S., Prentice, I. C., Barton, C. V. M., Crous, K. Y., de Angelis, P., Freeman, M., and Wingate, L.: Reconciling the Optimal and Empirical Approaches to Modelling Stomatal Conductance, Global Change Biology, 17, 2134–2144, https://doi.org/10.1111/j.1365-2486.2010.02375.x, 2011.

Ménard, C. B., Essery, R., Krinner, G., Arduini, G., Bartlett, P., Boone, A., Brutel-Vuilmet, C., Burke, E., Cuntz, M., Dai, Y., Decharme, B., Dutra, E., Fang, X., Fierz, C., Gusev, Y., Hagemann, S., Haverd, V., Kim, H., Lafaysse, M., Marke, T., Nasonova, O., Nitta, T., Niwano, M., Pomeroy, J., Schädler, G., Semenov, V. A., Smirnova, T., Strasser, U., Swenson, S., Turkov, D., Wever, N., and Yuan, H.: Scientific and Human Errors in a Snow Model Intercomparison, Bulletin of the American Meteorological Society, 102, E61–E79, https://doi.org/10.1175/BAMS-D-19-0329.1, 2021.

Milly, P. C. D.: Potential Evaporation and Soil Moisture in General Circulation Models, Journal of Climate, 5, 209–226, https://doi.org/10.1175/1520-0442(1992)005<0209:PEASMI>2.0.CO;2, 1992.

Modellbetreuungsgruppe: The ECHAM3 Atmospheric General Circulation Model, DKRZ Technical Report 6, Deutsches Klimarechenzentrum (DKRZ), Hamburg, Germany, 1994.

Moldrup, P., Olesen, T., Komatsu, T., Yoshikawa, S., Schjonning, P., and Rolston, DE.: Modeling Diffusion and Reaction in Soils: X. A Unifying Model for Solute and Gas Diffusivity in Unsaturated Soil, Soil Science, 168, 321–337, https://doi.org/10.1097/01.ss.0000070907.55992.3c, 2003.

Moldrup, P., Olesen, T., Yoshikawa, S., Komatsu, T., and Rolston, D. E.: Three-Porosity Model for Predicting the Gas Diffusion Coefficient in Undisturbed Soil, Soil Science Society of America Journal, 68, 750–759, https://doi.org/10.2136/sssaj2004.7500, 2004.

Müller, O. V., McGuire, P. C., Vidale, P. L., and Hawkins, E.: River Flow in the near Future: A Global Perspective in the Context of a High-Emission Climate Change Scenario, Hydrology and Earth System Sciences, 28, 2179–2201, https://doi.org/10.5194/hess-28-2179-2024, 2024.

Napoly, A., Boone, A., Samuelsson, P., Gollvik, S., Martin, E., Seferian, R., Carrer, D., Decharme, B., and Jarlan, L.: The Interactions between Soil–Biosphere–Atmosphere (ISBA) Land Surface Model Multi-Energy Balance (MEB) Option in SURFEXv8 – Part 2: Introduction of a Litter Formulation and Model Evaluation for Local-Scale Forest Sites, Geoscientific Model Development, 10, 1621–1644, https://doi.org/10.5194/gmd-10-1621-2017, 2017.

Nelson, J. A., Perez-Priego, O., Zhou, S., Poyatos, R., Zhang, Y., Blanken, P. D., Gimeno, T. E., Wohlfahrt, G., Desai, A. R., Gioli, B., Limousin, J.-M., Bonal, D., Paul-Limoges, E., Scott, R. L., Varlagin, A., Fuchs, K., Montagnani, L., Wolf, S., Delpierre, N., Berveiller, D., Gharun, M., Belelli-Marchesini, L., Gianelle, D., Šigut, L., Mammarella, I., Siebicke, L., Andrew Black, T., Knohl, A., Hörtnagl, L., Magliulo, V., Besnard, S., Weber, U., Carvalhais, N., Migliavacca, M., Reichstein, M., and Jung, M.: Ecosystem Transpiration and Evaporation: Insights from Three Water Flux Partitioning Methods across FLUXNET Sites, Global Change Biology, 26, 6916–6930, https://doi.org/10.1111/gcb.15314, 2020.

Nijssen, B., Bowling, L. C., Lettenmaier, D. P., Clark, D. B., El Maayar, M., Essery, R., Goers, S., Gusev, Y. M., Habets, F., Van Den Hurk, B., Jin, J., Kahan, D., Lohmann, D., Ma, X., Mahanama, S., Mocko, D., Nasonova, O., Niu, G.-Y., Samuelsson, P., Shmakin, A. B., Takata, K., Verseghy, D., Viterbo, P., Xia, Y., Xue, Y., and Yang, Z.-L.: Simulation of High Latitude Hydrological Processes in the Torne–Kalix Basin: PILPS Phase 2(e) 2: Comparison of Model Results with Observations, Global and Planetary Change, 38, 31–53, https://doi.org/10.1016/S0921-8181(03)00004-3, 2003.

Niu, G.-Y., Yang, Z.-L., Dickinson, R. E., and Gulden, L. E.: A Simple TOPMODEL-based Runoff Parameterization (SIMTOP) for Use in Global Climate Models, Journal of Geophysical Research: Atmospheres, 110, 2005JD006 111, https://doi.org/10.1029/2005JD006111, 2005.

https://doi.org/10.5194/egusphere-2026-4223
Preprint. Discussion started: 28 July 2026

Niu, G.-Y., Yang, Z.-L., Mitchell, K. E., Chen, F., Ek, M. B., Barlage, M., Kumar, A., Manning, K., Niyogi, D., Rosero, E., Tewari, M., and Xia, Y.: The Community Noah Land Surface Model with Multiparameterization Options (Noah-MP): 1. Model Description and Evaluation with Local-Scale Measurements, Journal of Geophysical Research, 116, D12 109, https://doi.org/10.1029/2010JD015139, 2011.

Noilhan, J. and Planton, S.: A Simple Parameterization of Land Surface Processes for Meteorological Models, Monthly Weather Review, 117, 536–549, 1989.

Ogée, J. and Brunet, Y.: A Forest Floor Model for Heat and Moisture Including a Litter Layer, Journal of Hydrology, 255, 212–233, https://doi.org/10.1016/S0022-1694(01)00515-7, 2002.

Philip, J. R.: Evaporation, And Moisture And Heat Fields In The Soil, Journal of Meteorology, 14, 354–366, 1957.

Reick, C. H., Gayler, V., Goll, D., Hagemann, S., Heidkamp, M., Nabel, J. E. M. S., Raddatz, T., Roeckner, E., Schnur, R., and Wilkenskjeld, S.: JSBACH 3 - The Land Component of the MPI Earth System Model: Documentation of Version 3.2, Reports on Earth System Science, Max Planck Institute for Meteorology, Hamburg, Germany, 240, 271, https://doi.org/10.17617/2.3279802, 2021.

Richards, L. A.: Capillary Conduction of Liquids through Porous Mediums, Journal of Applied Physics, 1, 318–333, https://doi.org/10.1063/1.1745010, 1931.

Robock, A., Schlosser, C., Vinnikov, K. Y., Speranskaya, N. A., Entin, J. K., and Qiu, S.: Evaluation of the AMIP Soil Moisture Simulations, Global and Planetary Change, 19, 181–208, https://doi.org/10.1016/S0921-8181(98)00047-2, 1998.

Rodell, M., Beaudoing, H. K., L'Ecuyer, T. S., Olson, W. S., Famiglietti, J. S., Houser, P. R., Adler, R., Bosilovich, M. G., Clayson, C. A., Chambers, D., Clark, E., Fetzer, E. J., Gao, X., Gu, G., Hilburn, K., Huffman, G. J., Lettenmaier, D. P., Liu, W. T., Robertson, F. R., Schlosser, C. A., Sheffield, J., and Wood, E. F.: The Observed State of the Water Cycle in the Early Twenty-First Century, Journal of Climate, 28, 8289–8318, https://doi.org/10.1175/JCLI-D-14-00555.1, 2015.

Sabot, M. E. B., De Kauwe, M. G., Pitman, A. J., Medlyn, B. E., Ellsworth, D. S., Martin-StPaul, N. K., Wu, J., Choat, B., Limousin, J.-M., Mitchell, P. J., Rogers, A., and Serbin, S. P.: One Stomatal Model to Rule Them All? Toward Improved Representation of Carbon and Water Exchange in Global Models, Journal of Advances in Modeling Earth Systems, 14, https://doi.org/10.1029/2021MS002761, 2022.

Sakaguchi, K. and Zeng, X.: Effects of Soil Wetness, Plant Litter, and under-Canopy Atmospheric Stability on Ground Evaporation in the Community Land Model (CLM3.5), Journal of Geophysical Research, 114, D01 107, https://doi.org/10.1029/2008JD010834, 2009.

Samaniego, L., Kumar, R., and Attinger, S.: Multiscale Parameter Regionalization of a Grid-Based Hydrologic Model at the Mesoscale, Water Resources Research, 46, W05 523, https://doi.org/10.1029/2008WR007327, 2010.

Samaniego, L., Kumar, R., Thober, S., Rakovec, O., Zink, M., Wanders, N., Eisner, S., Müller Schmied, H., Sutanudjaja, E. H., Warrach-Sagi, K., and Attinger, S.: Toward Seamless Hydrologic Predictions across Spatial Scales, Hydrology and Earth System Sciences, 21, 4323–4346, https://doi.org/10.5194/hess-21-4323-2017, 2017.

Samaniego, L., Thober, S., Wanders, N., Pan, M., Rakovec, O., Sheffield, J., Wood, E. F., Prudhomme, C., Rees, G., Houghton-Carr, H., Fry, M., Smith, K., Watts, G., Hisdal, H., Estrela, T., Buontempo, C., Marx, A., and Kumar, R.: Hydrological Forecasts and Projections for Improved Decision-Making in the Water Sector in Europe, Bulletin of the American Meteorological Society, 100, 2451–2472, https://doi.org/10.1175/BAMS-D-17-0274.1, 2019.

Saulnier, G.-M. and Datin, R.: Analytical Solution to a Bias in the TOPMODEL Framework Balance, Hydrological Processes, 18, 1195–1218, https://doi.org/10.1002/hyp.1346, 2004.

Schaake, J. C., Koren, V. I., Duan, Q. Y., Mitchell, K., and Chen, F.: Simple Water Balance Model for Estimating Runoff at Different Spatial and Temporal Scales, Journal of Geophysical Research: Atmospheres, 101, 7461–7475, https://doi.org/10.1029/95JD02892, 1996.

https://doi.org/10.5194/egusphere-2026-4223
Preprint. Discussion started: 28 July 2026

Schaap, M. G., Leij, F. J., and van Genuchten, M. T.: ROSETTA: A Computer Program for Estimating Soil Hydraulic Parameters with Hierarchical Pedotransfer Functions, Journal of Hydrology, 251, 163–176, https://doi.org/10.1016/S0022-1694(01)00466-8, 2001.

Schlesinger, W. H. and Jasechko, S.: Transpiration in the Global Water Cycle, Agricultural and Forest Meteorology, 189–190, 115–117, https://doi.org/10.1016/j.agrformet.2014.01.011, 2014.

Schweppe, R., Thober, S., Müller, S., Kelbling, M., Kumar, R., Attinger, S., and Samaniego, L.: MPR 1.0: A Stand-Alone Multiscale Parameter Regionalization Tool for Improved Parameter Estimation of Land Surface Models, Geoscientific Model Development, 15, 859–882, https://doi.org/10.5194/gmd-15-859-2022, 2022.

Sellers, P. J., Heiser, M. D., and Hall, F. G.: Relations between Surface Conductance and Spectral Vegetation Indeces at Intermediate (100 M2 to 15 Km2) Length Scales, Journal of Geophysical Research, 97, 19 033–19 059, 1992.

Sellers, P. J., Randall, D. A., Collatz, G. J., Berry, J. A., Field, C. B., Dazlich, DA., Zhang, C., Collelo, GD., and Bounoua, L.: A Revised Land Surface Parameterization (SiB2) for Atmospheric GCMs .1. Model Formulation, Journal of Climate, 9, 676–705, https://doi.org/10.1175/1520-0442(1996)009<0676:ARLSPF>2.0.CO;2, 1996.

Sitch, S., Friedlingstein, P., Gruber, N., Jones, S. D., Murray-Tortarolo, G., Ahlström, A., Doney, S. C., Graven, H., Heinze, C., Huntingford, C., Levis, S., Levy, P. E., Lomas, M., Poulter, B., Viovy, N., Zaehle, S., Zeng, N., Arneth, A., Bonan, G., Bopp, L., Canadell, J. G., Chevallier, F., Ciais, P., Ellis, R., Gloor, M., Peylin, P., Piao, S. L., Le Quéré, C., Smith, B., Zhu, Z., and Myneni, R.: Recent Trends and Drivers of Regional Sources and Sinks of Carbon Dioxide, Biogeosciences, 12, 653–679, https://doi.org/10.5194/bg-12-653-2015, 2015.

Sun, X., Wilcox, B. P., and Zou, C. B.: Evapotranspiration Partitioning in Dryland Ecosystems: A Global Meta-Analysis of in Situ Studies, Journal of Hydrology, 576, 123–136, https://doi.org/10.1016/j.jhydrol.2019.06.022, 2019.

Sutanudjaja, E. H., Van Beek, R., Wanders, N., Wada, Y., Bosmans, J. H. C., Drost, N., Van Der Ent, R. J., De Graaf, I. E. M., Hoch, J. M., De Jong, K., Karssenberg, D., López López, P., Peßenteiner, S., Schmitz, O., Straatsma, M. W., Vannametee, E., Wisser, D., and Bierkens, M. F. P.: PCR-GLOBWB 2: A 5 Arcmin Global Hydrological and Water Resources Model, Geoscientific Model Development, 11, 2429–2453, https://doi.org/10.5194/gmd-11-2429-2018, 2018.

Swenson, S. C. and Lawrence, D. M.: Assessing a Dry Surface Layer-based Soil Resistance Parameterization for the Community Land Model Using GRACE and FLUXNET-MTE Data, Journal of Geophysical Research: Atmospheres, 119, https://doi.org/10.1002/2014JD022314, 2014.

Tafasca, S., Ducharne, A., and Valentin, C.: Weak Sensitivity of the Terrestrial Water Budget to Global Soil Texture Maps in the ORCHIDEE Land Surface Model, Hydrology and Earth System Sciences, 24, 3753–3774, https://doi.org/10.5194/hess-24-3753-2020, 2020.

Takata, K., Emori, S., and Watanabe, T.: Development of the Minimal Advanced Treatments of Surface Interaction and Runoff, Global and Planetary Change, 38, 209–222, https://doi.org/10.1016/S0921-8181(03)00030-4, 2003.

van den Hurk, B., Kim, H., Krinner, G., Seneviratne, S. I., Derksen, C., Oki, T., Douville, H., Colin, J., Ducharne, A., Cheruy, F., Viovy, N., Puma, M. J., Wada, Y., Li, W., Jia, B., Alessandri, A., Lawrence, D. M., Weedon, G. P., Ellis, R., Hagemann, S., Mao, J., Flanner, M. G., Zampieri, M., Materia, S., Law, R. M., and Sheffield, J.: LS3MIP (v1.0) Contribution to CMIP6: The Land Surface, Snow and Soil Moisture Model Intercomparison Project – Aims, Setup and Expected Outcome, Geoscientific Model Development, 9, 2809–2832, https://doi.org/10.5194/gmd-9-2809-2016, 2016.

Van Looy, K., Bouma, J., Herbst, M., Koestel, J., Minasny, B., Mishra, U., Montzka, C., Nemes, A., Pachepsky, Y. A., Padarian, J., Schaap, M. G., Tóth, B., Verhoef, A., Vanderborght, J., van der Ploeg, M. J., Weihermüller, L., Zacharias, S., Zhang, Y., and Vereecken, H.: Pedotransfer Functions in Earth System Science: Challenges and Perspectives, Reviews of Geophysics, 55, 1199–1256, https://doi.org/10.1002/2017RG000581, 2017.

https://doi.org/10.5194/egusphere-2026-4223
Preprint. Discussion started: 28 July 2026

Vereecken, H., Weihermüller, L., Assouline, S., Šimůnek, J., Verhoef, A., Herbst, M., Archer, N., Mohanty, B., Montzka, C., Vanderborght, J., Balsamo, G., Bechtold, M., Boone, A., Chadburn, S., Cuntz, M., Decharme, B., Ducharne, A., Ek, M., Garrigues, S., Goergen, K., Ingwersen, J., Kollet, S., Lawrence, D. M., Li, Q., Or, D., Swenson, S., de Vrese, P., Walko, R., Wu, Y., and Xue, Y.: Infiltration from the Pedon to Global Grid Scales: An Overview and Outlook for Land Surface Modeling, Vadose Zone Journal, 18, 180 191, https://doi.org/10.2136/vzj2018.10.0191, 2019.

Wang, L., Good, S. P., and Caylor, K. K.: Global Synthesis of Vegetation Control on Evapotranspiration Partitioning, Geophysical Research Letters, 41, 6753–6757, https://doi.org/10.1002/2014GL061439, 2014.

Wankmüller, F. J. P., Delval, L., Lehmann, P., Baur, M. J., Cecere, A., Wolf, S., Or, D., Javaux, M., and Carminati, A.: Global Influence of Soil Texture on Ecosystem Water Limitation, Nature, 635, 631–638, https://doi.org/10.1038/s41586-024-08089-2, 2024.

Warszawski, L., Frieler, K., Huber, V., Piontek, F., Serdeczny, O., and Schewe, J.: The Inter-Sectoral Impact Model Intercomparison Project (ISI–MIP): Project Framework, Proceedings of the National Academy of Sciences, 111, 3228–3232, https://doi.org/10.1073/pnas.1312330110, 2014.

Weber, T. K. D., Weihermüller, L., Nemes, A., Bechtold, M., Degré, A., Diamantopoulos, E., Fatichi, S., Filipović, V., Gupta, S., Hohenbrink, T. L., Hirmas, D. R., Jackisch, C., De Jong Van Lier, Q., Koestel, J., Lehmann, P., Marthews, T. R., Minasny, B., Pagel, H., Van Der Ploeg, M., Shojaeezadeh, S. A., Svane, S. F., Szabó, B., Vereecken, H., Verhoef, A., Young, M., Zeng, Y., Zhang, Y., and Bonetti, S.: Hydro-Pedotransfer Functions: A Roadmap for Future Development, Hydrology and Earth System Sciences, 28, 3391–3433, https://doi.org/10.5194/hess-28-3391-2024, 2024.

Wei, Z., Yoshimura, K., Wang, L., Miralles, D. G., Jasechko, S., and Lee, X.: Revisiting the Contribution of Transpiration to Global Terrestrial Evapotranspiration, Geophysical Research Letters, 44, 2792–2801, https://doi.org/10.1002/2016GL072235, 2017.

Weihermüller, L., Lehmann, P., Herbst, M., Rahmati, M., Verhoef, A., Or, D., Jacques, D., and Vereecken, H.: Choice of Pedotransfer Functions Matters When Simulating Soil Water Balance Fluxes, Journal of Advances in Modeling Earth Systems, 13, e2020MS002 404, https://doi.org/10.1029/2020MS002404, 2021.

Wood, E. F., Lettenmaier, D. P., Liang, X., Lohmann, D., Boone, A., Chang, S., Chen, F., Dai, Y., Dickinson, R. E., Duan, Q., Ek, M., Gusev, Y. M., Habets, F., Irannejad, P., Koster, R., Mitchel, K. E., Nasonova, O. N., Noilhan, J., Schaake, J., Schlosser, A., Shao, Y., Shmakin, A. B., Verseghy, D., Warrach, K., Wetzel, P., Xue, Y., Yang, Z.-L., and Zeng, Q.-c.: The Project for Intercomparison of Land-Surface Parameterization Schemes (PILPS) Phase 2(c) Red–Arkansas River Basin Experiment: 1. Experiment Description and Summary Intercomparisons, Global and Planetary Change, 19, 115–135, https://doi.org/10.1016/S0921-8181(98)00044-7, 1998.

Yao, Y., Joetzjer, E., Ciais, P., Viovy, N., Cresto Aleina, F., Chave, J., Sack, L., Bartlett, M., Meir, P., Fisher, R., and Luyssaert, S.: Forest Fluxes and Mortality Response to Drought: Model Description (ORCHIDEE-CAN-NHA R7236) and Evaluation at the Caxiuanã Drought Experiment, Geoscientific Model Development, 15, 7809–7833, https://doi.org/10.5194/gmd-15-7809-2022, 2022.

Zeng, Y., Su, Z., Wan, L., and Wen, J.: A Simulation Analysis of the Advective Effect on Evaporation Using a Two-phase Heat and Mass Flow Model, Water Resources Research, 47, 2011WR010 701, https://doi.org/10.1029/2011WR010701, 2011.